

---

# COMPARATIVE ANALYSIS OF WEATHER-BASED INDEXES AND THE ACTUARIES CLIMATE INDEX™ FOR CROP YIELD PREDICTION AND WEATHER-DERIVATIVE PRICING

---

A PREPRINT

✉ **Cem Yavrum**

Institute of Applied Mathematics  
Middle East Technical University  
06800, Ankara, Türkiye  
cyavrum@metu.edu.tr

✉ **A. Sevtap Selcuk-Kestel**

Institute of Applied Mathematics  
Middle East Technical University  
06800, Ankara, Türkiye  
skestel@metu.edu.tr

✉ **José Garrido**

Concordia University  
Montreal, Canada  
jose.garrido@concordia.ca

October 31, 2025

## ABSTRACT

Climate change poses significant challenges to the agricultural and financial sectors, affecting crop productivity and overall financial stability. This study evaluates the robustness of the Actuaries Climate Index™ (ACI), a newer entrant in the field as a tool for measuring climate impacts, by comparing its explanatory power with well-established weather-based indexes (WBIs) across two key sectors. In the agricultural context, the yields of three major crops are predicted using generalized statistical models and advanced machine learning algorithms with climate indexes as explanatory variables. To enhance model reliability and address multicollinearity among weather-related variables, the study also incorporates both principal component analysis and functional principal component analysis. A total of 22 models, each constructed with different sets of explanatory variables, demonstrate the significant impact of wind speed and sea-level changes, alongside temperature and precipitation, on crop yield variability across six regions of the United States. For the financial market application, the analysis adapts the weather-derivative framework, as it is a critical instrument for energy companies, insurers, and agribusinesses seeking to hedge against weather-related risks. By analyzing the payoffs of derivative contracts that use WBIs and ACI components as underlying variables, the findings reveal that the ACI framework holds a strong potential as a comprehensive climate risk indicator, not only for the agricultural sector but also for the finance and insurance industries.

**Keywords** actuaries climate index · weather-derivative pricing · crop yield prediction · weather-based indexes · machine learning

## 1 Introduction

Climate change refers to long-term shifts in temperature and weather. Recent reports from the Intergovernmental Panel on Climate Change highlight the significant increase in global temperatures over the past few decades (IPCC 2022; Masson-Delmotte et al. 2021). The consequences of this warming extend across multiple domains, adversely affecting human health, global food security, financial stability, and the insurance industry. From a public health perspective, WHO (2014) project that climate change could lead to an additional 250,000 deaths per year between 2030 and 2050. In the financial sector, Gall et al. (2011) report that direct losses from natural hazards in the United States (U.S.) are steadily increasing and may reach between \$300 and \$400 billion within a single decade, driven by the increasing frequency and severity of extreme weather events. In terms of global food security, empirical studies by Lobell and Gourdji (2012), Hu et al. (2024), and Adhikari et al. (2015) demonstrate that the yields of major crops are significantly affected negatively by increasing temperatures and changing precipitation patterns. Similarly, within the insurance industry, Zhou et al. (2024) discuss the profound impact of climate change across various insurance sectors, underscoring the urgency for standardized methodologies to measure and quantify climate risks.

Climate impact is mostly measured and interpreted by indexes. In the literature, various indexes such as the Climate Extremes Index (Karl et al. 1996), Greenhouse Climate Response Index (Karl et al. 1996), Palmer Drought Severity Index (Palmer 1965), Cooling Degree Days (Jewson and Brix 2005), Heating Degree Days (Jewson and Brix 2005) and Cumulative Rainfall Index (Odening et al. 2007) are developed to quantify climate change, enabling researchers and policymakers to assess systematically its impact. In recent years, the Actuaries Climate Index<sup>TM</sup> (ACI) emerges as a pivotal tool for understanding and monitoring climate risks, offering valuable insights for insurance companies, governments, and the general public. Developed in 2016 by the four major North American actuarial societies, the ACI (2018) uses historical meteorological data from the U.S. and Canada to track extreme conditions in air temperature, precipitation, drought, wind, and sea-level rise.

The practical methodology of the ACI is quickly adapted for use in other countries. Curry (2015) demonstrates that the ACI framework is effectively applicable to regions like the United Kingdom and Europe. The Australian Actuaries Climate Index (AACI 2018), which is tailored to Australian meteorological conditions, is introduced, while Nevruz et al. (2022) develop the Turkish Actuaries Climate Index, specifically for the Ankara region in Türkiye. Similarly, Zhou et al. (2023) launch the Iberian Actuarial Climate Index, encompassing Spain and Portugal, marking the first application of the ACI framework to the European continent. Most recently, Garrido et al. (2023) and Rogo et al. (2025) extend this framework to France and Italy, respectively, creating the French and Italian Actuarial Climate Indexes. The continued international adoption of the ACI methodology demonstrates a growing global interest to quantifying, monitoring, and managing climate risks through standardized and comparable metrics.

Several studies in the literature also demonstrate the applicability of the ACI in various fields, particularly in insurance and finance. Jiang and Weng (2019) analyze ACI's predictive power for stock returns of agriculture-related companies in the U.S. and Canada, concluding that ACI could support a profitable trading strategy. Pan et al. (2022) assess ACI's effectiveness in predicting corn yields in the Midwest region of the U.S. using linear and probit regression models, finding satisfactory predictive power. Zhou and Vilar-Zanón (2024) explore the relationship between the Spanish Actuarial Climate Index and hailstorm-related insurance losses for grapes grown for wine producing, through linear and quantile regression models.

However, given its relatively recent addition, there remains a notable gap in the literature where a systematic evaluation of the ACI's predictive capability against traditional weather indexes would provide a significant contribution, thereby enhancing its applicability across broader fields and sectors. By comparing the explanatory power of the ACI with well-established weather-based indexes (WBIs) commonly used in the energy and derivatives markets, this study aims to evaluate the robustness of the ACI as a tool for measuring climate impacts in both the agricultural sector and financial markets. In the agricultural context, weather-based indexes are used to predict the yields of three major crops using regression models, namely Generalized Linear Model (GLM) and Generalized Additive Model (GAM), alongside advanced machine learning algorithms such as Extreme Gradient Boosting (XGB) and Light Gradient Boosting Machine (LGBM). For the financial market application, the analysis focuses on the payoffs of weather derivative contracts that use WBIs and ACI components as underlying variables. To the best of our knowledge, beyond comparing the ACI with traditional weather indexes, this study makes an additional novel contribution by presenting the first application of the ACI within a weather-derivative framework which is critical instrument for energy companies, insurers, and agribusinesses seeking effective hedging mechanisms against weather-related risks.

Regarding crop yield prediction, this study also investigates the individual contribution of each weather index to model performance by fitting 22 distinct models, each constructed with different sets of explanatory variables. Since all explanatory variables are weather-based, they may share common weather driven patterns, potentially leading to multicollinearity issues in regression models. Additionally, achieving comparable model performance with fewer explanatory variables is both practical and desirable. To address these challenges, dimension reduction techniques specifically, Principal Component Analysis (PCA) and Functional Principal Component Analysis (FPCA) are applied to identify the most influential variables in the data sets. This approach not only mitigates multicollinearity issues but also simplifies the models, improving efficiency and interpretability.

The findings of this paper demonstrate that both ACI components and traditional weather-based indexes exhibit robust predictive capabilities for crop yields. Furthermore, the inclusion of additional weather conditions such as drought, wind, and sea-level alongside conventional variables like air temperature and precipitation, substantially enhances model performance. Additionally, the high degree of consistency observed among the derivative payoffs underscores the ACI framework's potential as a comprehensive climate risk indicator, applicable not only to the agricultural sector but also to the finance and insurance industries.

The paper is organized as follows: Section 2 summarizes the climate indexes, whereas Section 3 describes the proposed methodology for predicting crop yields and pricing weather derivatives based on these indexes. The properties of the data and the results of the analyses are provided in Section 4. Finally, Section 5 concludes the paper by summarizing

the key findings and discussing their broader implications. Additional information on the regression models, machine learning algorithms, and dimensionality reduction techniques used in the analyses are provided in the Appendix A.

## 2 Climate Indexes

We focus on weather-based indexes, specifically Cooling Degree Days (CDD), Heating Degree Days (HDD), and the Cumulative Rainfall Index (PRE), which are directly linked to temperature and precipitation. These indexes hold particular advantages because they rely on a single weather variable, making them not only simple to interpret but also straightforward to compute. Their relative ease of use makes them especially suitable for comparative analyses with the components of the Actuaries Climate Index™. In the following subsections, the detailed formulations of these weather-based indexes and outlines of the corresponding components within the ACI framework are presented.

### 2.1 Weather-Based Indexes

CDD and HDD are temperature-based indexes, with CDD capturing warm weather conditions and HDD representing cool weather conditions. PRE, on the other hand, quantifies rainfall amounts. These indexes are initially calculated on a daily basis, and their values for longer intervals, such as monthly or meteorological seasons, are derived by summing the daily data. Briefly, CDD measures how much the daily average outside air temperature exceeds a base level temperature (usually taken as 65°F or 18°C), and HDD measures the opposite, the temperature falls below a base level (Jewson and Brix 2005).

Let  $T_i^{\max}$  and  $T_i^{\min}$  denote the maximum and minimum temperatures measured on day  $i$ . The average temperature for day  $i$  is defined as:

$$T_i = \frac{T_i^{\max} + T_i^{\min}}{2}. \quad (1)$$

If the average temperature is higher than 65°F for CDD and lower than 65°F for HDD, the differences for that day are calculated by:

$$CDD = \max\{T_i - 65, 0\}, \quad (2)$$

$$HDD = \max\{65 - T_i, 0\}, \quad (3)$$

respectively. Additionally, PRE represents the total volume of rainfall accumulated over a specified time period and is calculated by summing all daily rainfall measurements, expressed in millimeters (Odening et al. 2007):

$$PRE = \sum_{i=1}^L r_i, \quad (4)$$

where  $r_i$  denotes the daily total rainfall amount on day  $i$ , and  $L$  is the total number of days in the chosen time frame, such as a month or a meteorological season.

### 2.2 Actuaries Climate Index™

The ACI is designed to improve understanding of climate trends and their potential impact, incorporating various climate variables that signify extreme weather conditions. It comprises six components: high temperature (T90), low temperature (T10), precipitation (P), drought (D), wind speed (W), and sea-level (S). Since each component reflects different weather conditions, the ACI uses standardized values (anomalies) for all components to integrate them into a single index. Standardization is based on the mean and standard deviation of each component during the designated reference period of 1961 to 1990 (ACI 2018). The components of the ACI used in the analyses are defined as follows:

- (i) T90 represents the percentage of days in a month when daily temperatures exceed the 90th percentile of the corresponding days in the reference period.
- (ii) T10 reflects the percentage of days when daily temperatures fall below the 10th percentile of the reference period.
- (iii) P, denoted as Rx5day, measures the maximum amount of rainfall recorded over any five consecutive days within a month.

The standardized values of each component (anomalies) are computed both on a monthly and seasonal basis. For each month ( $j$ ) and year ( $q$ ), they are expressed as (Zhou et al. 2023):

$$T90_{STD}(j, q) = \frac{T90(j, q) - \mu_{T90(j)}}{\sigma_{T90(j)}}, \quad (5)$$

$$T10_{STD}(j, q) = \frac{T10(j, q) - \mu_{T10(j)}}{\sigma_{T10(j)}}, \quad (6)$$

$$P_{STD}(j, q) = \frac{Rx5day(j, q) - \mu_{Rx5day(j)}}{\sigma_{Rx5day(j)}}. \quad (7)$$

Here,  $\mu_{(\cdot)}$  and  $\sigma_{(\cdot)}$  are the mean and standard deviation of corresponding components for the reference period, respectively. The composite ACI is derived by averaging the standardized values of all six components, with the T10 component being assigned a negative value to account for its inverse relationship with warm weather conditions, and expressed as (ACI 2018):

$$ACI = \frac{T90_{STD} - T10_{STD} + P_{STD} + D_{STD} + W_{STD} + S_{STD}}{6}. \quad (8)$$

### 3 Proposed Methodology

Based on the main objectives, to evaluate the robustness of the ACI as a tool for measuring climate impacts in both the agricultural sector and financial markets, the study examines the performance of the ACI in two distinct applications: crop yield prediction as an agricultural case and the pricing of weather derivatives as a financial market case. Since the ACI is a relatively recent in the literature, its performance is compared against that of long-established weather-based indexes. By assessing the explanatory power of climate indexes, this study is expected to underscore the potential of the ACI for real-time applications and demonstrate its broader utility across diverse sectors.

#### 3.1 Crop Yield Prediction

The predictive capabilities of climate indexes on crop yields are evaluated using both traditional statistical models and modern machine learning algorithms. In the literature, regression models (Ansarifar et al. 2021; Shah et al. 2018; Shastri et al. 2017) and machine learning techniques (Crane-Droesch 2018; Iniyar et al. 2023; Mahesh and Soundrapandiyan 2024; Nigam et al. 2019; Van Klompenburg et al. 2020; You et al. 2017) are widely used for crop yield prediction, largely due to their ease of implementation, interpretability, and computational efficiency. In this study, the GLM and GAM, which are favored for their flexibility in handling distributional assumptions (detailed in Appendix A.1), are used. To complement these approaches and highlight the advantages of machine learning methods over traditional statistical models, two widely used gradient boosting algorithms, XGB and LGBM (detailed in Appendix A.2), are also incorporated.

Crop yields are influenced not only by weather conditions during the harvest period but also by extreme weather events occurring throughout the entire growing cycle, from planting to harvest. Adverse conditions such as temperature extremes and precipitation anomalies can have significant cumulative effects on crop development and productivity. To capture the full spectrum of potential impacts, the meteorological seasonal values of each index covering the entire year are included in the data sets. Additionally, the timing of harvest for each crop is carefully considered to ensure that the data sets encompass the complete year leading up to harvest, thereby reflecting all relevant weather impacts. The analyses fit a total of 22 models, each incorporating explanatory variables representing various weather measurements and their combinations. A detailed breakdown of each model and the associated data sets is presented in Table 1. Comprehensive information on the data sets, along with the crop yields fitted by each model, is provided in full in Section 4.

Despite differences in their calculation methods, the WBIs and ACI components can be systematically grouped based on the weather conditions they represent. Specifically, CDD (Eq. 2) and T90 (Eq. 5) both capture warm weather extremes, whereas HDD (Eq. 3) and T10 (Eq. 6) measure cold weather conditions. Similarly, PRE (Eq. 4) and P (Eq. 7) reflect the severity of precipitation. This classification provides a clear, logical, and consistent framework for comparing the indexes, ensuring a robust basis for evaluating their predictive power with respect to crop yields.

Table 1: Explanatory variables included in predicting crop yields

Model	Explanatory Variables	Model	Explanatory Variables	Model	Explanatory Variables
1	CDD	8	T90	15	T90-T10-P-W
2	HDD	9	T10	16	T90-T10-P-D
3	PRE	10	P	17	T90-T10-P-S
4	CDD-HDD	11	T90-T10	18	T90-T10-P-W-D
5	CDD-PRE	12	T90-P	19	T90-T10-P-W-S
6	HDD-PRE	13	T10-P	20	T90-T10-P-D-S
7	CDD-HDD-PRE	14	T90-T10-P	21	T90-T10-P-W-D-S
				22	ACI

The first seven models summarized in Table 1 are built using only WBIs and their combinations, providing a baseline for comparison. Models 8-14 replace these with ACI components that correspond one-to-one with the WBIs, enabling direct performance comparisons between the two index types. To extend the analysis, additional ACI components (W, D, S) that are not represented in the first 14 models are sequentially incorporated into Models 15-21. Finally, Model 22 uses the composite ACI, which aggregates all six components into a single index, offering a comprehensive measure of climate conditions.

A flowchart of the proposed methodology is presented in Figure 1. The framework consists of two distinct comparison structures designed to evaluate model performance under different input variables. In the first comparison analysis, the performance of regression models and machine learning algorithms is assessed using principal components derived from the explanatory variables. Since all indexes incorporated into the models are weather-based, they tend to reflect similar meteorological patterns, which may result in multicollinearity issues in regression analyses. To address this and simplify the explanatory data sets without compromising model accuracy, the PCA and FPCA (see details in Appendix A.3) are used as dimensionality reduction techniques. Comparing these two techniques also allows the performance evaluation of FPCA over PCA, particularly in modeling time-dependent data such as climate indexes.

Unlike regression models, machine learning algorithms do not require prior data simplification or the elimination of multicollinearity among variables. Therefore, the second comparison analysis directly uses the raw climate indexes as input variables into the machine learning algorithms, without applying any dimensionality reduction techniques. This approach not only allows for a direct assessment of model performance using the raw climate data but also provides a basis for evaluating the effectiveness of the principal component approach proposed in the methodology.

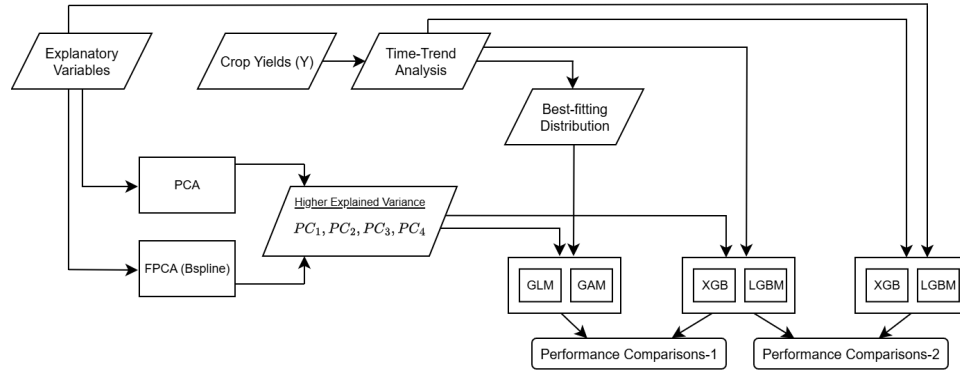


Figure 1: Flowchart of the proposed methodology

The Python packages “scikit-learn” (Fabian 2011) and “scikit-fda” (Ramos-Carreño et al. 2024) are used to implement PCA and FPCA with a B-spline basis, respectively. To maintain consistency and simplicity in model execution, the default settings of both packages are applied. From the transformed data sets, the first four principal components ( $PC_1$ ,  $PC_2$ ,  $PC_3$ ,  $PC_4$ ), which collectively account the majority of the variance in the data, are selected as the input variables for analyses.

### Time-Trend Analysis

In crop yield analysis, detrending time series is essential, as agricultural production often follows a long-term upward trend driven by technological innovations, and advances in farming practices. Without appropriately removing or controlling for the trend in time, predictive models especially regression-based approaches may overstate their

performance by simply capturing the persistent growth pattern instead of isolating the actual effects of weather and climate factors on yields.

A wide range of detrending techniques is available in the literature, including both parametric and non-parametric methods. Common approaches include linear trend (Zhou et al. 2021), quadratic trend (Bucheli et al. 2022), moving average smoothing (Lu et al. 2017), locally weighted regression (Lu et al. 2017), and two-knot linear spline (Liu and Ker 2021). In this study, the linear detrending method, the most widely used approach in agricultural economics, is adopted, as it offers both simplicity and interpretability. The detrended crop yields ( $Dy_t$ ) are defined as:

$$Dy_t = y_t - \hat{y}_t + \hat{y}_0, \quad (9)$$

where  $y_t$  represents the observed crop yields,  $\hat{y}_t$  denotes the values predicted from the fitted linear regression model, in which time  $t$  is used as the independent variable. The addition of  $\hat{y}_0$  ensures that all detrended yields are shifted to the level of the first predicted yield (Jewson and Brix 2005). This adjustment prevents the occurrence of negative values in the detrended series, which is particularly important because GLM and GAM with some specific link functions cannot accommodate negative-valued inputs. From Equation (9), the removed time trends ( $TT_t$ ) from the observed crop yields are obtained as follows:

$$TT_t = y_t - Dy_t = \hat{y}_t - \hat{y}_0. \quad (10)$$

The time stationarity of crop yields is evaluated using the Augmented Dickey-Fuller (ADF) test (Dickey and Fuller 1979), where the null hypothesis indicates that the crop yield series is non-stationary.

## Modeling

After detrending the crop yield data, the next crucial step is to determine both the appropriate distribution of the yields and the most suitable link function for GLMs and GAMs before performing regression analyses. The Python package “distfit” (Taskesen 2020) is used to identify the best-fitting distribution. This package evaluates 89 univariate distributions and selects the optimal one based on the residual sum of squares. For the link function, consistency across GLMs and GAMs is ensured by applying the log-link function in all models. The log-link function is particularly well-suited for crop yield data, as these values are inherently positive and continuous. The implementation of GLMs and GAMs is carried out using the R packages “stats” (Team 2022) and “mgcv” (Wood 2015), respectively. The GLM and GAM are expressed as:

$$\log(E(Dy|PC_1, PC_2, PC_3, PC_4)) = \beta_0 + \sum_{h=1}^4 \beta_h * PC_h, \quad (11)$$

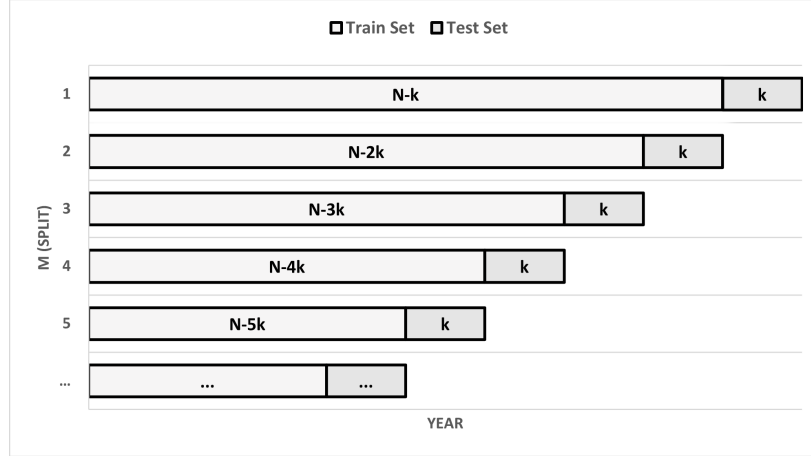
$$\log(E(Dy|PC_1, PC_2, PC_3, PC_4)) = \beta_0 + \sum_{h=1}^4 f_h(PC_h), \quad (12)$$

respectively. Here,  $Dy$  represents the detrended crop yields, and  $PC_h$  ( $h = 1, 2, 3, 4$ ) denote the principal components. The coefficients  $\beta_h$  are the model parameters, and  $f_h(\cdot)$  are smooth functions that capture potentially nonlinear relationships between principal components and the crop yields. In the analyses, both  $Dy$  and  $PC_h$  are treated as column vectors of size  $N \times 1$ , where  $N$  corresponds to the number of observations (years).

To construct the XGB and LGBM models, the Python packages “xgboost” (Brownlee 2019) and “lightgbm” (Microsoft 2017) are chosen among the alternatives, respectively. To maintain consistency, the same hyper-parameters are used in all models. These are the number of estimators (500), maximum depth (2), and learning rate (0.01).

## Cross-Validation

Given the time series nature of climate indexes, training and test sets cannot be selected randomly when applying cross-validation methods. A random split would create the unrealistic situation in which future data points are used to predict past values. Therefore, we apply the iterative *M-split leave-k-out cross-validation* method, which is specifically suitable for time series applications. In this approach, the data set is divided into  $M$  sequential splits, where each test set contains a unique block of  $k$  consecutive observations. By iteratively leaving out these  $k$  observations for testing, while the preceding observations are used for training, the method ensures that the natural time order is preserved. The cross-validation procedure applied in this study is illustrated in Figure 2.

Figure 2:  $M$ -split leave- $k$ -out cross-validation method

In the procedure,  $M$  is the number of splits,  $N$  denotes the total number of observations (years), while  $k$  is set to approximately 10% of  $N$ . Accordingly, the train/test share for the first iteration (split) is arranged as 90% training data and 10% testing data. Model performance is assessed on both training and test sets using the Mean Absolute Percentage Error (MAPE). The models are fitted to the detrended crop yields; however, the removed time trends are reintroduced during performance evaluation to ensure that predictive accuracy reflects the true scale of observed yields. The overall MAPE of the model across all splits for the training and test sets are:

$$MAPE_{Train} = \frac{1}{M} \sum_{m=1}^M \left[ \frac{1}{N - mk} \sum_{t=1}^{N-mk} \frac{|y_t - \hat{D}y_t + TT_t|}{y_t} \right], \quad (13)$$

$$MAPE_{Test} = \frac{1}{M} \sum_{m=1}^M \left[ \frac{1}{k} \sum_{t=N-mk+1}^{N-mk+k} \frac{|y_t - \hat{D}y_t + TT_t|}{y_t} \right], \quad (14)$$

respectively. Here,  $y_t$  denotes the observed crop yields,  $\hat{D}y_t$  represents the predicted detrended crop yields, and  $TT_t$  corresponds to the removed time trends, where  $t$  indicates time (year).

### 3.2 Weather-Derivative Pricing

For the financial market application, the similarities between WBIs and the components of the ACI are examined by evaluating the strength of their correlations and comparing their empirical cumulative distribution function (ECDF) values. The comparison is structured across three groups, each representing a different type of weather condition, thereby enabling a systematic and detailed comparison of the indexes. Mainly, the focus is on testing the performances of indexes within the weather-derivative framework and comparing their outcomes. For this purpose, the payoffs of weather derivative contracts are analyzed using underlying variables derived from both the WBIs and ACI components. This approach permits to investigate whether the indexes exhibit similar financial performance in market-based applications, thereby extending their potential utility beyond the agricultural sector.

#### Index Comparison

The grouping of indexes, established to enable meaningful comparisons, is summarized in Table 2. The time periods assigned to each group (Group 1: Summer, Group 2: Winter, Group 3: Spring) are carefully selected to align with the practical applications of climate indexes. For example, CDD is widely used to estimate energy demand during the summer cooling season, whereas HDD is frequently used to assess heating requirements in the winter (Spinoni et al. 2018). Regarding precipitation, its timing plays a critical role in agricultural productivity. Wang et al. (2016) highlight that crop yields are especially sensitive to rainfall during the rainy season, whereas Peltonen-Sainio et al. (2011) show that precipitation before harvest often negatively impacts crop yields. Therefore, for the precipitation group, index comparisons are conducted for the spring months to encompass the rainy season preceding the general harvest period of most crops.

Table 2: Structure of groups

Group	Weather-Based Indexes (WBIs)	Components of the ACI	Meteorological Season	Measurement
1	CDD	T90	Summer	Warm weather
2	HDD	T10	Winter	Cool weather
3	PRE	P	Spring	Precipitation

The dependence between the indexes is analyzed using the Spearman rank correlation coefficient (Zar 2005), while distributional comparisons are conducted through the Anderson-Darling (A-D) test (Anderson and Darling 1954). The A-D test is chosen over the more commonly known Kolmogorov-Smirnov test because the former is more sensitive to the tails of the distribution (Engmann and Cousineau 2011), making it particularly suitable in applications involving climate indexes, where extreme weather conditions often play a critical role in determining outcomes.

### Derivative Contracts

Weather derivatives are structured in several contract forms based on different underlying weather indexes. In the literature, the most commonly used indexes are CDD, HDD, and PRE (Odening et al. 2007; Solanilla Blanco 2025). Regarding contract types, the most frequent forms are call/put options, and swaps (Alaton et al. 2002; Jewson and Brix 2005). Basically, a call option provides a payout when the underlying weather index exceeds a predefined threshold, whereas a put option triggers a payout if the index falls below that threshold. Swaps, on the other hand, are structured as agreements between two parties to exchange cash flows based on the difference between the actual observed weather outcomes and an agreed-upon strike level. In this study, an uncapped call option is used, whose payoff  $PO$  is defined as follows:

$$PO = \alpha \max\{I - K, 0\}, \quad (15)$$

where  $I$  represents the value of the underlying weather index, and  $K$  denotes the predetermined strike level. Here,  $\alpha$  is the tick size, specifying the monetary value assigned per unit of the index.

### Pricing Methods

Pricing of weather derivatives involves determining a fair contract value using one of several methods. Two commonly used ones, which are also adopted in this study, are the **Historical Burn Analysis (HBA)** and **Index Modeling (IM)** (Alexandridis and Zapranis 2012). The HBA is widely used as a benchmark because of its simplicity, since it does not require fitting a probability distribution to the weather index or solving complex stochastic equations. The idea behind HBA is retrospective: it evaluates how the contract would have been performed in previous years and estimates the expected future payoff as the average of historical payoffs. The fair price of a call option under HBA can be computed with the following steps:

- (i) Determine the fair strike level ( $K$ ) using historical weather index values.
- (ii) Calculate the historical payoffs of the option for each year based on the observed index values.
- (iii) Compute the mean of the historical payoffs, which serves as a fair price.

Alternatively, within the IM method, the underlying weather index can be directly modeled to estimate the fair price of derivative contracts. The IM relies on statistical and stochastic representations of the weather index to construct its probability distribution, from which the expected payoff is derived. Once the distribution of the weather index is identified and its parameters are estimated, simulated index values are generated to compute expected payoffs. Similar to the HBA method, the mean of these simulated payoffs represents the fair price of the contract.

## 4 Empirical Analysis

Each component of the ACI consists of a time series, either on a monthly basis, or for meteorological seasons (three-month periods ending in February, May, August, and November). These time series, starting in 1961, are derived from measurements collected at meteorological stations across the U.S. and Canada. The data sets are constructed separately for each country, in combination, and across 12 sub-regions. This study uses the U.S. data, where states are grouped into seven sub-regions based on their geographic locations: Alaska (ALA), Central East Atlantic (CEA), Central West Pacific (CWP), Midwest (MID), Southeast Atlantic (SEA), Southern Plains (SPL), and Southwest Pacific (SWP). The analyses use standardized seasonal values for each of the six ACI components (T90, T10, P, D, W, S) as well as the

composite index (ACI). This seasonal data, obtained from the official Actuaries Climate Index™ website<sup>1</sup>, cover a 64-year period from 1961 to 2024 for all seven sub-regions.

Regarding weather-based indexes, the National Oceanic and Atmospheric Administration (NOAA) Climate database<sup>2</sup> provides monthly data on CDD, HDD, and PRE for all U.S. states, covering the period from 1895 to the present. To align with the ACI data, seasonal values for CDD, HDD, and PRE between 1961 and 2024 are calculated by summing the monthly values for each meteorological season. Sub-regional data is subsequently generated by averaging the seasonal values of all states within each region. However, due to the unavailability of CDD and HDD data for Alaska, the analyses are performed on the six remaining regions of the U.S.

Annual crop yield data (in bushels per acre) for three major agricultural products-corn (grain), wheat (winter), and soybeans-produced in the U.S. is obtained from USDA's National Agricultural Statistical Service (NASS) Quick Stats portal<sup>3</sup> for all states, covering the period from 1961 to 2024. Following the same approach used in regional weather-based index calculations, sub-regional crop yields are calculated by averaging the annual yields of the states within each region. Analyses for corn and wheat are conducted across all regions, while for soybeans, due to data limitations, the analyses are restricted to four regions: CEA, CWP, MID, and SEA.

The climate impacts of weather-based indexes and ACI components on the agricultural and financial markets are analyzed using data from six U.S. regions, and the corresponding findings are presented.

#### 4.1 Agricultural Case

Firstly, the explanatory variables in each model (Table 1) are transformed into their principal components using PCA and FPCA. Figure 3 illustrates the total variation in the data sets, represented as regional averages, explained by the first four principal components derived from both methods for each model. The results demonstrate that the total variance explained by FPCA consistently surpasses that of PCA across all models, highlighting FPCA's superior performance when dealing with time-dependent data sets like climate indexes.

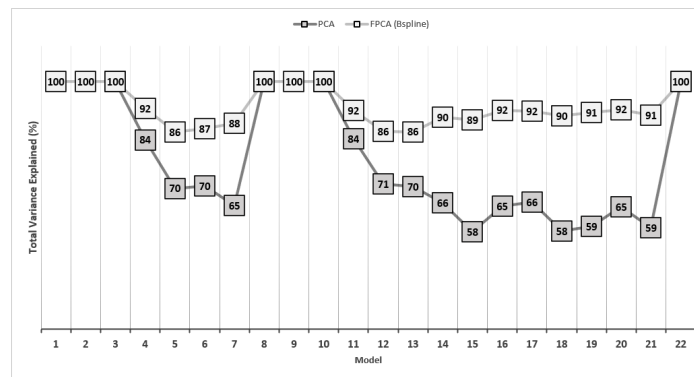


Figure 3: Explained variance comparisons of PCA and FPCA as regional averages

Upon closer examination of Figure 3, the models (1, 2, 3, 8, 9, 10, and 22) show a total explained variance of 100% for both PCA and FPCA. This is expected, as these models contain only one explanatory variable represented by its four seasonal values. Consequently, PCA and FPCA serve purely as data transformation tools for these cases without affecting the total variance explained.

For a detailed comparison, recall that the first seven models are constructed based on WBIs, while the subsequent seven models (Models 8-14) use their ACI counterparts. When comparing the total explained variance between these paired models (e.g., 1 vs. 8, 2 vs. 9, 3 vs. 10, and so forth), it is clear that the values are nearly equivalent. For instance, PCA explains 70% of the variance in Model 5, whereas it explains 71% in Model 12. Similarly, FPCA captures 88% of the variance in Model 7 and 90% in Model 14. Since the choice of explanatory variables, and consequently the derived principal components, directly affects the outcomes of the analyses, ensuring high and comparable explained variance values across both index groups is crucial for robustness. Given that FPCA consistently accounts for a larger proportion of variance across all models, with values exceeding 85%, the FPCA-derived principal components are selected for the subsequent analyses, ensuring better model accuracy and reliability.

<sup>1</sup>ACI website: <https://actuariesclimateindex.org/data/>

<sup>2</sup>NOAA database: <https://www.ncei.noaa.gov/access/monitoring/products/>

<sup>3</sup>NASS Quick Stats: <https://quickstats.nass.usda.gov/>

Secondly, potential time trends in the crop yields are examined using the ADF test, and where necessary, the yields are detrended using Equation (9). The regional ADF test results for all crops are summarized in Table 3, where  $p$ -values below 0.05 indicate that the data are time-stationary. As shown in Table 3, only the SPL and SWP regions for corn are initially found to be stationary; therefore, no transformation is applied to the data in these regions. The repeated ADF test results obtained after detrending confirm that all crop yields become time-stationary. The detrended crop yields, illustrated for each region in Figure 4, are then used as the dependent variables in the regression and machine learning analyses.

Table 3: Regional ADF test results for each crop

ADF test ( $p$ -value)	Crop	Region					
		CEA	CWP	MID	SEA	SPL	SWP
Before Detrend	Corn	0.997	0.787	0.971	0.902	0.045	0.033
	Wheat	0.959	0.314	0.996	0.996	0.546	0.181
	Soybeans	0.717	-	0.993	0.961	0.994	-
After Detrend	Corn	<0.01	0.049	<0.01	<0.01	-	-
	Wheat	<0.01	<0.01	0.038	<0.01	<0.01	0.047
	Soybeans	<0.01	-	<0.01	0.041	<0.01	-



Figure 4: Detrended crop yields over time

Thirdly, to establish a solid foundation for crop yields using GLMs and GAMs, the best-fitting distribution from the exponential family is identified using detrended crop yields for all regions. The resulting distributions are presented in Table 4. The incorporation of region-specific distributions ensures that the regression models account for spatial variability in crop yields, further improving the precision and relevance of the analyses.

Table 4: Best-fitting distributions for each crop

Region	Crop		
	Corn	Wheat	Soybeans
CEA	gamma	normal	gamma
CWP	gamma	normal	-
MID	gamma	gamma	gamma
SEA	normal	normal	gamma
SPL	normal	gamma	gamma
SWP	normal	normal	-

Before obtaining the performance results of the models, the parameters for cross-validation are set as  $N = 64$ ,  $M = 5$ , and  $k = 6$  in Equations (13) and (14). The MAPE values as regional averages for the training data of each crop are presented in Table 5. Based on the average values presented in the last row of Table 5, the GAM performs slightly better than the GLM, achieving lower MAPE values, though the difference remains relatively small. A similar pattern is observed between the XGB and LGBM, where XGB consistently outperforms LGBM, ultimately producing the lowest MAPE values among all methods. For the training data set, the average error rates for XGB range between 4% and 6% across all crops, whereas for LGBM, this range increases to 8%-15%. In contrast, the regression-based models exhibit significantly higher error rates, approximately around 30%.

Table 5: MAPE values as regional averages for each crop, model and method (Train set)

Model	Corn				Wheat				Soybeans			
	GLM	GAM	XGB	LGBM	GLM	GAM	XGB	LGBM	GLM	GAM	XGB	LGBM
1	0.362	0.345	0.071	0.154	0.282	0.278	0.047	0.089	0.297	0.298	0.039	0.084
2	0.364	0.358	0.080	0.161	0.283	0.276	0.047	0.089	0.295	0.296	0.049	0.090
3	0.383	0.374	0.079	0.166	0.283	0.281	0.042	0.086	0.295	0.296	0.038	0.084
4	0.359	0.357	0.075	0.153	0.282	0.279	0.048	0.088	0.295	0.296	0.043	0.086
5	0.365	0.345	0.071	0.157	0.282	0.278	0.044	0.086	0.294	0.295	0.035	0.082
6	0.356	0.340	0.064	0.154	0.282	0.281	0.040	0.083	0.294	0.293	0.038	0.086
7	0.349	0.348	0.069	0.152	0.281	0.277	0.040	0.084	0.293	0.293	0.039	0.084
8	0.368	0.351	0.075	0.153	0.285	0.283	0.047	0.089	0.296	0.297	0.041	0.085
9	0.368	0.355	0.077	0.161	0.283	0.281	0.048	0.089	0.297	0.296	0.045	0.087
10	0.369	0.352	0.074	0.161	0.280	0.280	0.043	0.085	0.294	0.292	0.043	0.089
11	0.364	0.336	0.072	0.155	0.283	0.282	0.048	0.088	0.295	0.295	0.043	0.086
12	0.357	0.345	0.066	0.148	0.278	0.275	0.039	0.084	0.294	0.294	0.041	0.084
13	0.353	0.347	0.066	0.147	0.279	0.277	0.040	0.083	0.294	0.295	0.046	0.086
14	0.350	0.339	0.063	0.150	0.279	0.275	0.040	0.085	0.294	0.294	0.044	0.088
15	0.356	0.350	0.070	0.150	0.279	0.277	0.043	0.085	0.294	0.293	0.042	0.088
16	0.347	0.341	0.062	0.149	0.280	0.276	0.038	0.083	0.292	0.292	0.045	0.089
17	0.336	0.325	0.054	0.130	0.280	0.280	0.040	0.084	0.293	0.293	0.043	0.086
18	0.351	0.340	0.068	0.153	0.280	0.277	0.041	0.082	0.292	0.292	0.045	0.088
19	0.335	0.312	0.052	0.138	0.279	0.280	0.043	0.085	0.294	0.294	0.043	0.087
20	0.332	0.314	0.050	0.137	0.280	0.278	0.040	0.084	0.292	0.291	0.040	0.086
21	0.336	0.314	0.054	0.143	0.279	0.276	0.044	0.085	0.291	0.290	0.044	0.087
22	0.357	0.342	0.071	0.151	0.285	0.284	0.045	0.089	0.293	0.292	0.049	0.091
Avg.	<b>0.355</b>	<b>0.342</b>	<b>0.067</b>	<b>0.151</b>	<b>0.281</b>	<b>0.279</b>	<b>0.043</b>	<b>0.086</b>	<b>0.294</b>	<b>0.294</b>	<b>0.042</b>	<b>0.087</b>

Since the GLM and GAM yield unsatisfactory results for the training set and XGM consistently outperforms LGBM, the MAPE values as regional averages for the test set are reported only for XGB in Figure 5. However, for a more comprehensive comparison across models, the regional MAPE values computed separately for both training and test data sets for all crops are given in Tables B2-B5 of the Appendix.

For corn, Model 19 achieves the best performance with a MAPE of 8.3%. The results of each model facilitate a detailed examination of how individual ACI components influence crop yields. For instance, Model 14, which includes temperature and precipitation components (T90, T10, P), achieves a MAPE of 10.4%. Sequentially adding the wind (W), drought (D), and sea-level (S) components in Models 15, 16, and 17, respectively, allows to evaluate their incremental effects. Among these, Model 17 produces the best result with a MAPE of 8.4%, indicating that the sea-level component has the strongest positive effect on corn yield prediction, reducing the error from 10.4% to 8.4%. Furthermore, when the wind and sea-level components are combined (Model 19), model performance improves slightly further, reaching 8.3% MAPE. Interestingly, Model 21, which incorporates all six ACI components, performs worse than Model 19. This outcome suggests that while wind and sea-level components enhance predictive accuracy, the inclusion of the drought has a diminishing effect on model performance when all other five climate variables of ACI are already used as predictors.

For wheat, similar to the findings for corn, Model 19 achieves the best overall performance, yielding a MAPE of 8.2%. When examining the individual component models, Model 8 (T90), Model 9 (T10), and Model 10 (P) produce MAPE values of 9.2%, 8.7%, and 8.4%, respectively. These results indicate that, when analyzed individually, precipitation has a relatively higher impact on wheat yield prediction than the temperature-related components. When precipitation is combined with low-temperature extremes (as in Model 13), model's performance improves slightly, with the MAPE decreasing to 8.3%. Furthermore, considering Models 15 (9.2%), 16 (8.8%), and 17 (8.7%), which sequentially incorporate wind, drought, and sea-level components, alongside temperature and precipitation, the results reveal that the sea-level component contributes the most substantial improvement in predictive accuracy.

For soybeans, the results differ slightly from those obtained for corn and wheat. The best-performing model for soybeans is Model 17 (MAPE of 7.5%). Unlike the findings for the other two crops, the inclusion of the wind component appears to negatively affect model performance for soybean yield. The performance difference between Model 12 (T90 and P) and Model 13 (T10 and P) is noteworthy. Model 12 achieves a MAPE of 8.2%, while Model 13 yields a higher error of 8.9%, indicating that warm weather extremes (T90) appear to have a stronger influence on soybean yield than cold weather extremes (T10). This conclusion is further supported by the performance results of Model 8 (T90: 8.4%) and Model 9 (T10: 9.2%).

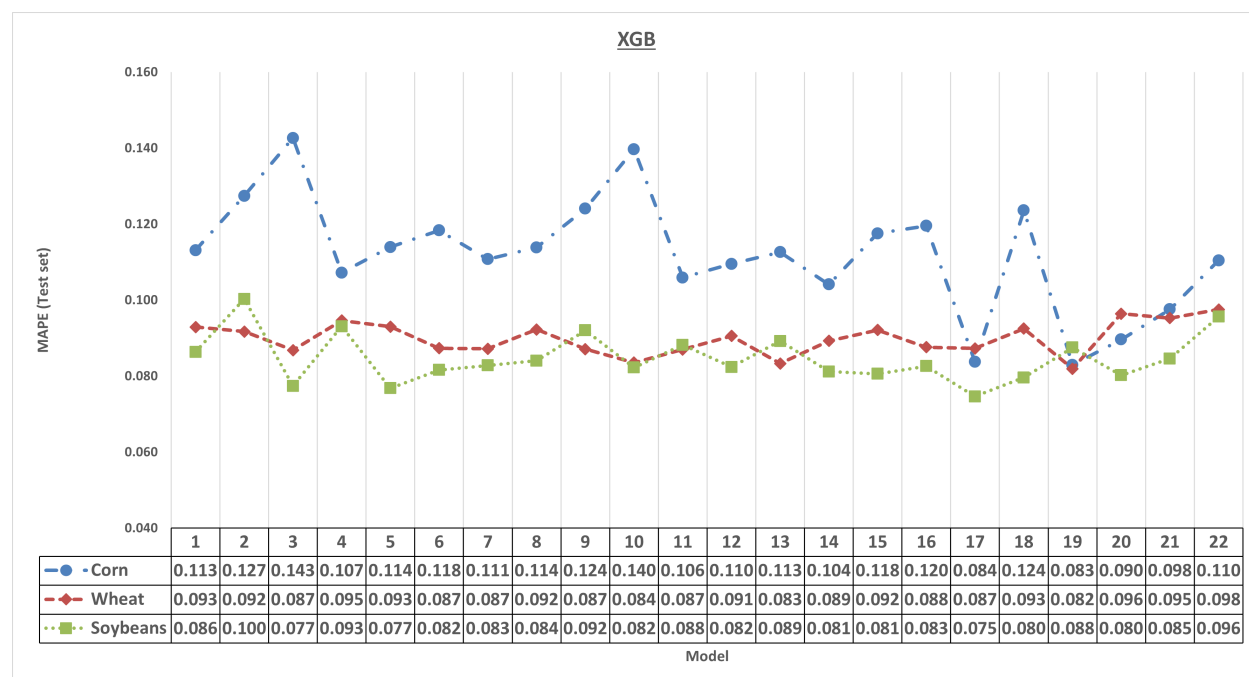


Figure 5: MAPE values as regional averages for each crop and model with XGB (Test set)

When analyzing the best-performing models for the three crops (Model 19 for corn and wheat, Model 17 for soybeans), it becomes clear that, alongside the temperature and precipitation components, sea-level change plays a significant role in yield prediction. One possible explanation for this is that variations in sea-level can impact crop productivity more broadly through mechanisms such as increased soil salinity, flooding, and the loss of agricultural land. Furthermore, wind appears to have a less pronounced effect on soybean yield compared to corn and wheat, likely due to the relatively short stature of soybean plants, which makes them more resistant to wind-induced damage. In contrast, taller crops like corn and wheat are more vulnerable to lodging<sup>4</sup> and other wind-related stresses that can negatively impact their overall yield.

A detailed comparison of the performance results for paired models (1 vs. 8, 2 vs. 9, 3 vs. 10, and so forth) on crop yields also reveals consistent and satisfactory outcomes. For instance, the performance difference between Model 1 (CDD: 11.3%) and Model 8 (T90: 11.4%) for corn, Model 2 (HDD: 9.2%) and Model 9 (T10: 8.7%) for wheat, Model 3 (PRE: 7.7%) and Model 10 (P: 8.2%) for soybeans are almost negligible, suggesting comparable explanatory power between ACI components and their WBI counterparts.

Another critical observation is that Model 22, which uses the composite ACI by aggregating all six components into a single index, consistently underperforms compared to Model 21, which incorporates each component separately, across all crops. These results emphasize that the composite ACI alone fails to fully capture and explain the complex weather conditions affecting crop yields. Consequently, analyzing the individual components separately provides a more nuanced and effective modeling approach, leading to improved accuracy in predicting yield variations.

The second comparison in the analysis (see Figure 1) is designed to evaluate the performance sensitivity of machine learning algorithms with respect to different input variables. In Table 6, XGB refers to the results obtained using principal components derived from climate indexes, while XGB-C corresponds to the scenario where the climate indexes are directly used as input variables. Notably, with the XGB-C method, Model 21, which constitutes the largest data set,

<sup>4</sup>Lodging refers to the bending or collapse of crop stems, often caused by strong winds, which makes harvesting difficult.

consistently yields the best performance, with only a slight difference compared to the second-best models. Among the remaining models that exclude one or more components, the second-best performing models remain consistent with those from the first comparison analysis (Model 19 for corn and wheat, Model 17 for soybeans). One possible explanation for this is that the direct use of climate indexes preserves all original information in the data sets, enabling machine learning algorithms to process and use a greater number of features more effectively, compared to the more compressed data sets derived through principal component analysis. Regional performance metrics of XGB-C are also given in Table B6 of the Appendix.

Table 6: Performance Comparison-2: MAPE values as regional averages for each crop (Test set)

Model	Corn		Wheat		Soybeans	
	XGB	XGB-C	XGB	XGB-C	XGB	XGB-C
1	0.113	0.103	0.093	0.092	0.086	0.085
2	0.127	0.134	0.092	0.091	0.100	0.100
3	0.143	0.149	0.087	0.086	0.077	0.072
4	0.107	0.107	0.095	0.090	0.093	0.086
5	0.114	0.103	0.093	0.086	0.077	0.075
6	0.118	0.125	0.087	0.084	0.082	0.073
7	0.111	0.106	0.087	0.085	0.083	0.077
8	0.114	0.102	0.092	0.089	0.084	0.087
9	0.124	0.126	0.087	0.088	0.092	0.099
10	0.140	0.140	0.084	0.085	0.082	0.082
11	0.106	0.106	0.087	0.085	0.088	0.089
12	0.110	0.105	0.091	0.084	0.082	0.083
13	0.113	0.113	0.083	0.087	0.089	0.085
14	0.104	0.105	0.089	0.084	0.081	0.082
15	0.118	0.110	0.092	0.087	0.081	0.080
16	0.120	0.115	0.088	0.086	0.083	0.084
17	0.084	0.087	0.087	0.085	<b>0.075*</b>	<b>0.068<sup>φ</sup></b>
18	0.124	0.118	0.093	0.084	0.080	0.080
19	<b>0.083*</b>	<b>0.078<sup>φ</sup></b>	<b>0.082*</b>	<b>0.084<sup>φ</sup></b>	0.088	0.074
20	0.090	0.085	0.096	0.088	0.080	0.078
21	0.098	<b>0.075*</b>	0.095	<b>0.082*</b>	0.085	<b>0.068*</b>
22	0.110	0.096	0.098	0.094	0.096	0.094

Note. \* Best results, <sup>φ</sup> Second best results.

## 4.2 Financial Market Case

The analysis of weather derivatives pricing begins by examining the dependence among the three groups (see Table 2). Table 7 presents the correlation coefficients ( $\rho$ ) between the weather-based indexes and their corresponding ACI components within each group, along with the  $p$ -values from the A-D test, which evaluates the null hypothesis that the two distributions are identical. Despite methodological differences in constructing the indexes, strong positive correlations are observed between the corresponding indexes. For the A-D test,  $p$ -values greater than 0.05 (bold in Table 7) indicate that the paired indexes exhibit statistically similar distributions. The results show that the precipitation-related indexes in Group-3 tend to display similar distributions across most regions compared to temperature-based indexes analyzed in the first two groups. Detailed descriptive statistics for each group are provided in Table B1 of the Appendix.

Table 7: Similarity tests within each group

		Region					
		CEA	CWP	MID	SEA	SPL	SWP
Group-1 (CDD-T90)	$\rho$	0.88	0.90	0.89	0.94	0.86	0.97
	A-D test ( $p$ -value)	0.040	<0.01	<0.01	<0.01	<0.01	<b>0.250</b>
Group-2 (HDD-T10)	$\rho$	0.89	0.83	0.86	0.87	0.81	0.80
	A-D test ( $p$ -value)	0.025	<0.01	<0.01	<0.01	<b>0.105</b>	<0.01
Group-3 (PRE-P)	$\rho$	0.83	0.79	0.88	0.87	0.69	0.84
	A-D test ( $p$ -value)	<b>0.250</b>	<b>0.126</b>	<b>0.250</b>	<b>0.189</b>	<0.01	<b>0.085</b>

Note.  $\rho$ : Spearman rank correlation coefficient.

For the payoff analysis of derivative options, pairs of indexes with the highest and lowest correlations are selected as case studies. As shown in Table 7, the pair with the strongest correlation is identified in Group-1 for the SWP region ( $\rho = 0.97$ ), while the weakest correlation is found in Group-3 for the SPL region ( $\rho = 0.69$ ). Call option payoffs are calculated using Equation (15), based on the index values from these two groups and regions.

Additionally, the key assumption of the HBA and IM pricing methods, which is that the underlying index should be time-stationary, is also considered. According to the ADF test results (not shown), the CDD and T90 indexes in Group-1 for the SWP region are determined to be non-stationary; therefore, these series are detrended using Equation (9) prior to inclusion in the analyses.

For consistency, the tick size ( $\alpha$ ) in the Equation (15) is set to 100 for both groups, and the strike level ( $K$ ) is defined as the mean of the historical index values plus 20% of their standard deviation (Jewson and Brix 2005). In the HBA method, payoffs for each year are computed, and the correlations between the payoffs and their A-D test results are analyzed. For the IM method, the best-fitting distributions for the historical indexes are identified, and 1,000 index values are simulated from these distributions to compute payoffs. Finally, the A-D test is applied to the simulated payoffs values. The results of the similarity tests comparing the payoffs obtained from both methods are summarized in Table 8.

Table 8: Similarity tests between payoffs for each method

Method	N	Compared Parameters		Group-1 (SWP)		Group-3 (SPL)	
				CDD	T90	PRE	P
HBA	64	Payoffs	$\rho$	0.82	0.65		
			A-D test ( $p$ -value)	0.250	0.250		
IM	64	Indexes	Best-fitting dist.	weibull	beta	lognorm	weibull
	1,000	Payoffs	A-D test ( $p$ -value)	<0.01		0.038	

Note.  $\rho$ : Spearman rank correlation coefficient, N: Number of years.

According to Table 8, the correlations among the payoffs obtained using the HBA method closely align with the correlations observed between the original indexes. For Group-1 (SWP), the correlation coefficient between the payoffs is 0.82 (down from 0.97), while for Group-3 (SPL), it is 0.65 (decreasing from 0.69). The decline observed for Group-1 (SWP) is expected, as the CDD and T90 indexes are detrended prior to the analysis. Moreover, based on the A-D test results for the HBA method ( $p > 0.05$ ), the payoff distributions are statistically similar. Interestingly, although the A-D test results for Group-3 (SPL) in Table 7 show no distributional similarity between the indexes themselves, the observed similarity among their payoffs implies that these indexes exhibit consistent behavior in terms of financial outcomes, highlighting their potential applicability in weather-derivative markets.

Table 8 reports the best-fitting distributions for each index pair (with detrended CDD and T90). Distinct best-fitting distributions are identified for all indexes, a finding further confirmed by the A-D test results derived from 1,000 simulated indexes and their corresponding payoffs ( $p < 0.05$ ). In contrast to the HBA findings, no similar distributions are detected among the simulated payoffs in the IM approach, indicating that the degree of similarity among payoffs in simulation-based analyses strongly depends on the distributional characteristics of the underlying indexes themselves.

The payoffs and ECDF values derived from both methods are illustrated in Figure 6. Examination of the payoff graphs reveals that the call options constructed from the indexes within each group often generate payments during similar time periods. This pattern indicates that the indexes tend to reach extreme values simultaneously, confirming their consistency and suitability for use in weather-derivative markets.

The fair price of uncapped call option can be determined through the HBA method by averaging all historical payoffs. For Group-1, the fair price is calculated as 2,192.23 for CDD and 34.74 for T90. Similarly, for Group-3, the corresponding fair prices are 36.34 for PRE and 40.61 for P. The observed discrepancies in fair prices arise from the fact that each index expresses weather conditions using different measurement units. Recall that CDD quantifies temperature in degree-days, whereas PRE measures precipitation in millimeters. In contrast, the ACI components T90 and P express weather conditions as standardized deviations relative to a reference period. Comparing the prices obtained using T90 and P, which share identical units, indicates that the call option priced with P is more expensive than that based on T90 (40.61 vs. 34.74). This finding suggests that extreme precipitation events have historically occurred more frequently than extreme temperature events.

## 5 Concluding Remarks

This study investigates the Actuaries Climate Index™ within both the agricultural and financial sectors, comparing its effectiveness with widely recognized weather-based indexes. In the agricultural context, the analysis focuses on evaluating the predictive capabilities of ACI components and traditional WBIs for three major crops. By fitting 22 distinct models, each constructed with different combinations of climate indexes, the study examines the individual and joint contributions of each weather index to overall model performance. For the financial market application, the analysis centers on the payoffs of weather derivative contracts that use WBIs and ACI components as underlying variables. By assessing the strength of correlations among payoffs and comparing their ECDF values, the study evaluates the potential of these indexes for broader financial use.

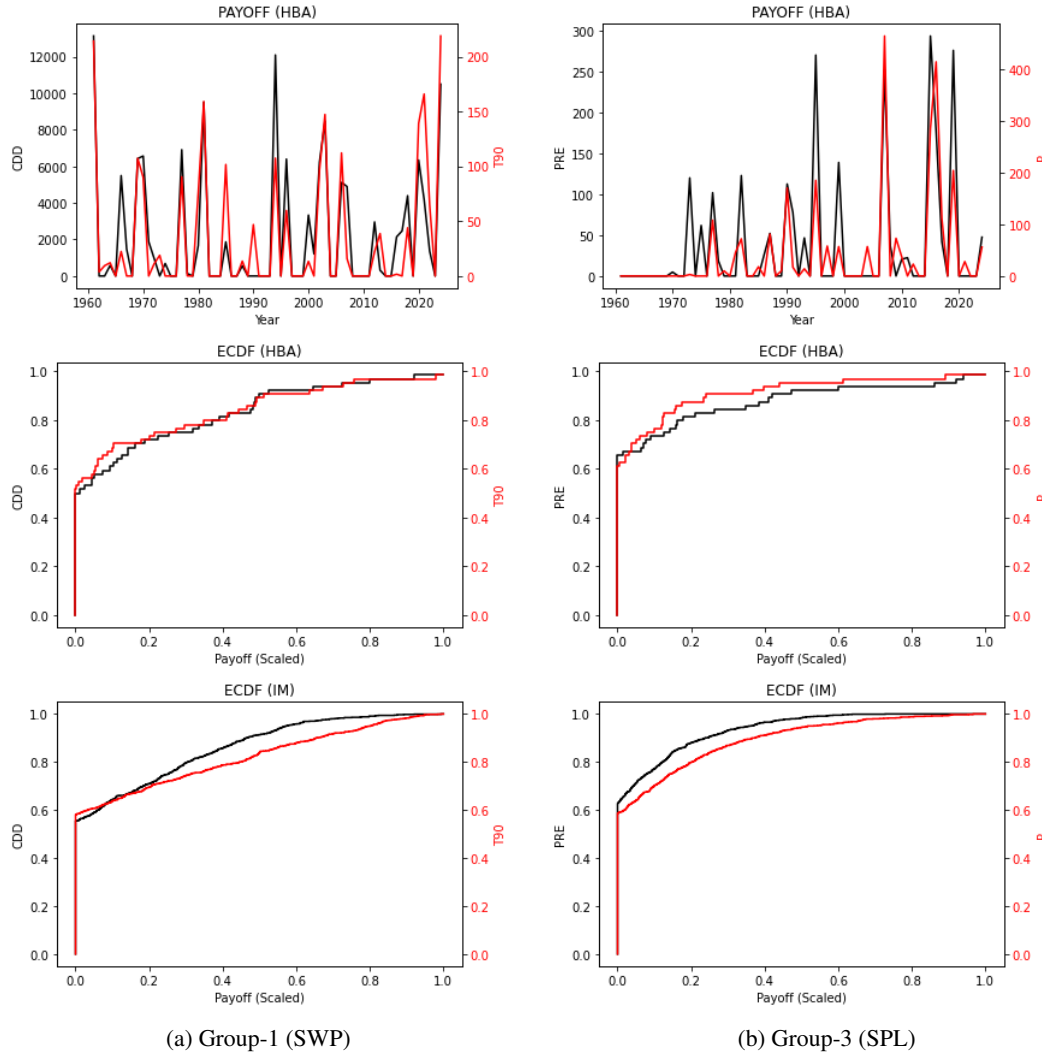


Figure 6: Payoffs and ECDF values for each method

Overall, based on the low MAPE values achieved in crop yield modeling and the consistency observed among the derivative payoffs, the results indicate that climate indexes demonstrate strong predictive performance and stable financial behavior. These findings highlight their applicability as effective climate risk indicators in both agricultural forecasting and weather-derivative markets. The key insights drawn from the analyses can be summarized as follows:

- (i) The FPCA consistently outperforms the traditional PCA in terms of explanatory variance, when applied to time-dependent climate indexes.
- (ii) The four principal components derived through FPCA effectively capture the underlying patterns in crop yield variations.
- (iii) The ACI components and their WBI counterparts exhibit strong correlation, and deliver similar predictive performance in predicting crop yields, especially with machine learning algorithms.
- (iv) The inclusion of indexes representing additional weather conditions-such as wind speed, and sea-level changes-alongside temperature and precipitation, improves model performance.
- (v) The composite ACI index alone fails to fully capture and explain the complex weather conditions affecting crop yields.
- (vi) The ACI components and their WBI counterparts generate similar derivative payoffs during comparable time periods, particularly when evaluated using the HBA method.

The outcomes suggest that the ACI framework holds strong potential as a comprehensive climate risk indicator, not only for the agricultural sector but also for the finance and insurance industries, where climate-related metrics are increasingly critical for risk assessment and decision-making.

Despite the promising performance metrics achieved, the study can be further improved in several aspects. One notable limitation is that regional crop yields are assessed by averaging the annual yields of the states within each region. This approach overlooks the fact that some states may have a greater influence on regional agricultural output due to their size or productivity levels. Moreover, the selection of the best-performing models for each crop is based on regional average results, which may not accurately reflect optimal performance at the regional or state level. Consequently, identifying and evaluating the best models for each specific region or state would enhance the precision and applicability of the findings, particularly for targeted applications in the insurance sector.

The proposed methodology also contributes to the literature on forecasting crop yields. Forecasting weather-related factors that significantly impact crop yields such as temperature, precipitation, and sea-level, often requires complex, time-consuming methods due to their inherently dynamic nature. However, by incorporating future projections of components derived through the FPCA method, crop yield forecasts can be achieved in a more efficient and convenient manner.

From a financial perspective, the study further encourages the broader adoption of the Actuaries Climate Index<sup>TM</sup> in risk management and hedging strategies. Demonstrating its applicability within weather-derivative framework underscores its potential utility for energy companies, insurers, and agribusinesses seeking to mitigate exposure to weather-related risks.

## Acknowledgments

Jose Garrido gratefully acknowledges the financial support of the Natural Sciences and Engineering Research Council of Canada (RGPIN-2017-06643).

## References

- AACI. *Design Documentation: Australian Actuaries Climate Index*. The Institute of Actuaries, Australia, 2018. Available online: <https://www.actuaries.asn.au/microsites/climate-index/about/development-and-design> (last accessed on 18 April 2025).
- ACI. *Actuaries Climate Index: Development and Design*. American Academy of Actuaries, the Canadian Institute of Actuaries, the Casualty Actuarial Society, and the Society of Actuaries, 2018. Available online: <https://actuariesclimateindex.org/wp-content/uploads/2019/05/ACI.DevDes.2.20.pdf> (last accessed on 18 April 2025).
- Umesh Adhikari, A Pouyan Nejadhashemi, and Sean A Woznicki. Climate change and eastern africa: a review of impact on major crops. *Food and Energy Security*, 4(2):110–132, 2015.
- Peter Alaton, Boualem Djehiche, and David Stillberger. On modelling and pricing weather derivatives. *Applied Mathematical Finance*, 9(1):1–20, 2002.
- Antonis Alexandridis and Achilleas D Zapranis. *Weather derivatives: modeling and pricing weather-related risk*. Springer Science & Business Media, 2012.
- Theodore W Anderson and Donald A Darling. A test of goodness of fit. *Journal of the American Statistical Association*, 49(268):765–769, 1954.
- Javad Ansarifard, Lizhi Wang, and Sotirios V Archontoulis. An interaction regression model for crop yield prediction. *Scientific Reports*, 11(1):17754, 2021.
- Jason Brownlee. Xgboost with python. *Machine Learning Mastery*, 2019.
- Janic Bucheli, Tobias Dalhaus, and Robert Finger. Temperature effects on crop yields in heat index insurance. *Food Policy*, 107:102214, 2022.
- Tianqi Chen and Carlos Guestrin. Xgboost: A scalable tree boosting system. In *Proceedings of the 22nd acm sigkdd international conference on knowledge discovery and data mining*, pages 785–794, 2016.
- Andrew Crane-Droesch. Machine learning methods for crop yield prediction and climate change impact assessment in agriculture. *Environmental Research Letters*, 13(11):114003, 2018.
- Charles L. Curry. Extension of the actuaries climate index to the uk and europe. *A Feasibility Study*. Institute and Faculty of Actuaries, 2015.

- David A Dickey and Wayne A Fuller. Distribution of the estimators for autoregressive time series with a unit root. *Journal of the American Statistical Association*, 74(366a):427–431, 1979.
- Sonja Engmann and Denis Cousineau. Comparing distributions: the two-sample anderson-darling test as an alternative to the kolmogorov-smirnov test. *Journal of Applied Quantitative Methods*, 6(3), 2011.
- Pedregosa Fabian. Scikit-learn: Machine learning in python. *Journal of Machine Learning Research* 12, page 2825, 2011.
- Melanie Gall, Kevin A Borden, Christopher T Emrich, and Susan L Cutter. The unsustainable trend of natural hazard losses in the united states. *Sustainability*, 3(11):2157–2181, 2011.
- José Garrido, Xavier Milhau, and Anani Olympio. The definition of a french actuarial climate index; one more step towards a european index. 2023.
- Trevor J Hastie. Generalized additive models. *Statistical Models in S*, pages 249–307, 2017.
- Harold Hotelling. Analysis of a complex of statistical variables into principal components. *Journal of Educational Psychology*, 24(6):417, 1933.
- Tongxi Hu, Xuesong Zhang, Sami Khanal, Robyn Wilson, Guoyong Leng, Elizabeth M Toman, Xuhui Wang, Yang Li, and Kaiguang Zhao. Climate change impacts on crop yields: A review of empirical findings, statistical crop models, and machine learning methods. *Environmental Modelling & Software*, page 106119, 2024.
- Shanmugam Iniyan, Vegesna Akhil Varma, and Ch Teja Naidu. Crop yield prediction using machine learning techniques. *Advances in Engineering Software*, 175:103326, 2023.
- IPCC. *Climate Change 2022: Impacts, Adaptation, and Vulnerability*. Cambridge University Press, 2022. Available online: <https://www.ipcc.ch/report/sixth-assessment-report-working-group-ii/> (last accessed on 18 April 2025).
- Stephen Jewson and Anders Brix. *Weather derivative valuation: the meteorological, statistical, financial and mathematical foundations*. Cambridge University Press, 2005.
- Ruihong Jiang and Chengguo Weng. Climate change risk and agriculture-related stocks. Available at SSRN 3506311, 2019.
- Thomas R Karl, Richard W Knight, David R Easterling, and Robert G Quayle. Indices of climate change for the united states. *Bulletin of the American Meteorological Society*, 77(2):279–292, 1996.
- Guolin Ke, Qi Meng, Thomas Finley, Taifeng Wang, Wei Chen, Weidong Ma, Qiwei Ye, and Tie-Yan Liu. Lightgbm: A highly efficient gradient boosting decision tree. *Advances in Neural Information Processing Systems*, 30, 2017.
- Yong Liu and Alan P Ker. Simultaneous borrowing of information across space and time for pricing insurance contracts: An application to rating crop insurance policies. *Journal of Risk and Insurance*, 88(1):231–257, 2021.
- David B Lobell and Sharon M Gourdj. The influence of climate change on global crop productivity. *Plant Physiology*, 160(4):1686–1697, 2012.
- Junyu Lu, Gregory J Carbone, and Peng Gao. Detrending crop yield data for spatial visualization of drought impacts in the united states, 1895–2014. *Agricultural and Forest Meteorology*, 237:196–208, 2017.
- Pavithra Mahesh and Rajkumar Soundrapandian. Yield prediction for crops by gradient-based algorithms. *Plos One*, 19(8):e0291928, 2024.
- Valérie Masson-Delmotte, Panmao Zhai, Anna Pirani, Sarah L Connors, Clotilde Péan, Sophie Berger, Nada Caud, Y Chen, L Goldfarb, MI Gomis, et al. Climate change 2021: the physical science basis. *Contribution of Working Group I to the Sixth Assessment Report of the Intergovernmental Panel on Climate Change*, 2(1):2391, 2021.
- Microsoft. *LightGBM Python-package*, 2017. Available online: <https://github.com/microsoft/LightGBM/tree/master/python-package> (last accessed on 18 April 2025).
- John Ashworth Nelder and Robert WM Wedderburn. Generalized linear models. *Journal of the Royal Statistical Society Series A: Statistics in Society*, 135(3):370–384, 1972.
- Ezgi Nevruz, Raif Yakup Atıcı, and Kasirga Yildirak. Actuaries climate index: An application for turkey. *İstatistik Araştırma Dergisi*, 12(2):14–25, 2022.
- Aruvansh Nigam, Saksham Garg, Archit Agrawal, and Parul Agrawal. Crop yield prediction using machine learning algorithms. In *2019 fifth international conference on image information processing (ICIIP)*, pages 125–130. IEEE, 2019.
- Martin Odening, Oliver Mußhoff, and Wei Xu. Analysis of rainfall derivatives using daily precipitation models: Opportunities and pitfalls. *Agricultural Finance Review*, 67(1):135, 2007.
- Wayne C Palmer. Meteorological drought. us. *Weather Bureau Res. Paper*, 45:1–58, 1965.

- Qimeng Pan, Lysa Porth, and Hong Li. Assessing the effectiveness of the actuaries climate index for estimating the impact of extreme weather on crop yield and insurance applications. *Sustainability*, 14(11):6916, 2022.
- Karl Pearson. Liii. on lines and planes of closest fit to systems of points in space. *The London, Edinburgh, and Dublin Philosophical Magazine and Journal of Science*, 2(11):559–572, 1901.
- Pirjo Peltonen-Sainio, Lauri Jauhiainen, and Kaija Hakala. Crop responses to temperature and precipitation according to long-term multi-location trials at high-latitude conditions. *The Journal of Agricultural Science*, 149(1):49–62, 2011.
- Carlos Ramos-Carreño, José Luis Torrecilla, Miguel Carbajo-Berrocal, Pablo Marcos, and Alberto Suárez. scikit-fda: a python package for functional data analysis. *Journal of Statistical Software*, 109:1–37, 2024.
- James O Ramsay and Bernard W Silverman. *Applied functional data analysis: methods and case studies*. Springer, 2002.
- Barbara Rogo, José Garrido, and Stefano Demartis. The italian actuarial climate index: A national implementation within the emerging european framework. *Risks*, 2025.
- Ayush Shah, Akash Dubey, Vishesh Hemnani, Divye Gala, and DR Kalbande. Smart farming system: Crop yield prediction using regression techniques. In *Proceedings of International Conference on Wireless Communication: ICWiCom 2017*, pages 49–56. Springer, 2018.
- Han Lin Shang. A survey of functional principal component analysis. *AStA Advances in Statistical Analysis*, 98: 121–142, 2014.
- Aditya Shastry, HA Sanjay, and E Bhanusree. Prediction of crop yield using regression techniques. *International Journal of Soft Computing*, 12(2):96–102, 2017.
- Sara Solanilla Blanco. Local sensitivity analysis of heating degree day and cooling degree day temperature derivative prices. *Quantitative Finance*, 25(4):653–670, 2025.
- Jonathan Spinoni, Jürgen V Vogt, Paulo Barbosa, Alessandro Dosio, Niall McCormick, Andrea Bigano, and Hans-Martin Füssl. Changes of heating and cooling degree-days in europe from 1981 to 2100. *Int. J. Climatol*, 38(51): e191–e208, 2018.
- Erdogan Taskesen. distfit is a python library for probability density fitting., Jan 2020. URL <https://erdogant.github.io/distfit>.
- R Development Core Team. R: A language and environment for statistical computing. 2022.
- Thomas Van Klompenburg, Ayalew Kassahun, and Cagatay Catal. Crop yield prediction using machine learning: A systematic literature review. *Computers and Electronics in Agriculture*, 177:105709, 2020.
- Xiaobin Wang, Dianxiong Cai, Huijun Wu, WB Hoogmoed, and O Oenema. Effects of variation in rainfall on rainfed crop yields and water use in dryland farming areas in china. *Arid Land Research and Management*, 30(1):1–24, 2016.
- WHO. Quantitative risk assessment of the effects of climate change on selected causes of death, 2030s and 2050s. In *Quantitative risk assessment of the effects of climate change on selected causes of death, 2030s and 2050s*. 2014.
- Simon Wood. Package ‘mgcv’. *R Package Version*, 1(29):729, 2015.
- Simon N Wood. *Generalized additive models: an introduction with R*. chapman and hall/CRC, 2017.
- Jiaxuan You, Xiaocheng Li, Melvin Low, David Lobell, and Stefano Ermon. Deep gaussian process for crop yield prediction based on remote sensing data. In *Proceedings of the AAAI conference on artificial intelligence*, volume 31, 2017.
- Jerrold H Zar. Spearman rank correlation. *Encyclopedia of Biostatistics*, 7, 2005.
- Nan Zhou and José L Vilar-Zanón. Impact assessment of climate change on hailstorm risk in spanish wine grape crop insurance: Insights from linear and quantile regressions. *Risks*, 12(2):20, 2024.
- Nan Zhou, José Luis Vilar-Zanón, José Garrido, and Antonio-José Heras Martínez. On the definition of an actuarial climate index for the iberian peninsula. In *Anales del Instituto de Actuarios Españoles*, number 29, pages 37–59, 2023.
- Nan Zhou, José Luis Vilar-Zanón, Jose Garrido, and Antonio José Heras-Martínez. Measuring climate change from an actuarial perspective: a survey of insurance applications. *Global Policy*, 15:34–46, 2024.
- Wang Zhou, Kaiyu Guan, Bin Peng, Zhuo Wang, Rong Fu, Bo Li, Elizabeth A Ainsworth, Evan DeLucia, Lei Zhao, and Zhangliang Chen. A generic risk assessment framework to evaluate historical and future climate-induced risk for rainfed corn and soybean yield in the us midwest. *Weather and Climate Extremes*, 33:100369, 2021.

## Appendix

### A Preliminaries

In this section, an overview of Generalized Linear Models (GLMs) and Generalized Additive Models (GAMs), which belong to the class of generalized statistical models, as well as Extreme Gradient Boosting (XGB) and Light Gradient Boosting Machine (LGBM), which are classified as machine learning algorithms, is provided. Furthermore, the Principal Component Analysis (PCA) and Functional Principal Component Analysis (FPCA), two dimensionality reduction techniques used to preprocess and simplify data sets before being incorporated into the models, are reviewed.

#### A.1 Generalized Statistical Models

GLMs are widely used regression framework that extends traditional linear models by accommodating response variables with error distributions other than normal (Nelder and Wedderburn 1972). It is applied in various fields due to its flexibility. Simply, the model setting consists of three key components: a distribution, a linear predictor, and a link function. The general formulation of GLMs is:

$$g(E(Y|X)) = X\beta, \quad (16)$$

where  $Y$  represents the response variable, chosen from the exponential family (e.g., Binomial, Poisson, or Gaussian). The linear predictor can be expressed as  $\eta = X\beta$ , where  $X$  is the matrix of independent variables, and  $\beta$  is the coefficient vector. The link function  $g(\cdot)$  connects the conditional expectation of  $Y$  to the linear predictor. Commonly used link functions, depending on the chosen distribution, are the identity, logarithmic and logistic functions.

While the GLMs are powerful and widely used tool for estimation and prediction, they have some limitations. One significant drawback is their assumption of a linear relationship between the predictors and the response variable. When the true relationship is non-linear, the results of GLMs can become biased or yield inaccurate predictions. GAMs address this limitation by extending the GLMs framework to accommodate non-linear relationships (Hastie 2017; Wood 2017). GAMs relax the linearity assumption by replacing linear terms with smooth functions, enabling each predictor to have its own potentially non-linear effect on the response variable. In general, the GAMs take the form:

$$g(E(Y|X)) = \eta = \beta_0 + f_1(X_1) + f_2(X_2) + \dots + f_p(X_p), \quad (17)$$

where  $\beta_0$  is the intercept term, and  $f_h(X_h)$  ( $h = 1, \dots, p$ ) are smooth functions that model the non-linear effects of the predictors  $X_h$  on the response variable. The flexibility of GAMs allow them to capture complex relationships while retaining interpretability, making it an effective tool for modeling real-world problems with non-linear dependencies.

#### A.2 Machine Learning Algorithms

XGB is an advanced implementation of the gradient boosting framework, optimized for performance and computational efficiency (Chen and Guestrin 2016). It is a well-optimized and scalable algorithm that is particularly suitable for regression, classification (binary and multiclass), and ranking problems. The algorithm functions by adding weak learners, such as decision trees, to the ensemble iteratively, with each successive model trying to correct the errors of the previous models. It uses a regularized objective function that includes both the training loss and a penalty term to control model complexity and avoid overfitting. The regularized objective can be written as:

$$\mathcal{L}^{(t)} = \sum_{i=1}^n \ell \left( y_i, \hat{y}_i^{(t-1)} + f_t(x_i) \right) + \Omega(f_t), \quad \text{where} \quad \Omega(f) = \gamma T + \frac{1}{2} \lambda \|\mathbf{w}\|^2. \quad (18)$$

Here,  $\ell$  denotes a differentiable loss function,  $\hat{y}_i^{(t-1)}$  is the prediction at iteration  $t - 1$ ,  $\Omega(f_t)$  penalizes the complexity of each tree  $f_t$ , with  $T$  being the number of leaves and  $\mathbf{w}$  the vector of leaf weights.

On the other hand, LGBM is a gradient boosting framework designed for speed and efficiency, especially on large-scale data sets with high dimensionality (Ke et al. 2017). It uses Gradient-based One-Side Sampling which selectively retains instances with large gradients to better capture under-fitted samples. Unlike level-wise growth used in other tree-based models, LGBM adopts a leaf-wise tree growth strategy that expands the leaf with the largest loss reduction, which often leads to lower loss with fewer iterations. The model minimizes the following objective function:

$$L(\theta) = \sum_{i=1}^n \ell(y_i, \hat{y}_i) + \sum_{j=1}^K \Omega(f_j), \quad (19)$$

where  $L(\theta)$  is the total loss,  $n$  is the number of samples,  $K$  is the number of trees, and  $\Omega(f_j)$  is a regularization term that penalizes the complexity of the model to avoid overfitting.

### A.3 Dimensionality Reduction in Modeling

For high dimensional explanatory variables, it is important to be able to reduce the number of variables while preserving valuable information as best possible. Simplifying the data set enhances interpretability, reduces computational complexity, and minimizes redundancy and noise. One widely used method for dimension reduction is principal component analysis. PCA transforms the original variables into a new set of uncorrelated variables called principal components (Hotelling 1933; Pearson 1901). Standardization is needed when the variables in the data set are on different scales.

Given a data matrix  $X$  of size  $n \times p$  where  $n$  represents the number of observations and  $p$  is the number of variables, each element in  $X$  can be standardized around its mean value, normalized by its standard deviation, thus obtaining a matrix of  $Z$ . PCA seeks to find the principal components by calculating the eigenvectors and eigenvalues of the covariance matrix,  $\Sigma_{p \times p}$ , given by:

$$\Sigma = \frac{1}{n-1} Z^T Z. \quad (20)$$

Singular value decomposition (SDV) is then applied to decompose the covariance matrix,  $\Sigma$ . The eigenvalue equation is expressed as:

$$\Sigma V = \lambda V, \quad (21)$$

where  $\lambda_{p \times p}$  is a diagonal matrix consisting of the set of all eigenvalues of  $\Sigma$  along its principal diagonal, and zero for all other elements, and  $V_{p \times p}$  is the matrix consisting of all eigenvectors of  $\Sigma$ , one eigenvector per column. The component with the largest eigenvalue becomes the first principal component which explains the greatest variation in the data. The explained variance,  $\sigma_{EXP}^2$ , by first  $k$  eigenvalues is then calculated by:

$$\sigma_{EXP}^2 = \frac{\sum_{j=1}^k \lambda_j}{\sum_{j=1}^p \lambda_j}. \quad (22)$$

The order of the data points in the data set analyzed by PCA has no impact on the results. This is because PCA treats the data set as a collection of vectors and does not account for the sequential or spatial arrangement of the data; the order can be permuted without altering the outcome. This makes PCA unsuitable for analyzing functional data, such as time series or curves, where the sequence of observations holds critical information. Functional principal component analysis extends traditional PCA, tailoring it to analyze data where each observation is a continuous function defined over some domain, rather than a discrete vector (Ramsay and Silverman 2002; Shang 2014).

Let  $F(t)$  denote functional data defined over a domain  $t \in [a, b]$ , where  $t$  represents time. Then, functional data can be represented using a basis function expansion, expressed as:

$$F(t) = \sum_{k=1}^{\infty} \beta_k \phi_k(t) + \epsilon(t), \quad (23)$$

where  $\phi_k(t)$  are the eigenfunctions (e.g., B-splines, Fourier or monomial basis),  $\beta_k$  are the coefficients associated with each functional principal component, and  $\epsilon(t)$  represents noise. Instead of a covariance matrix, FPCA uses a covariance function  $C(s, t)$  for decomposition. The eigenfunctions  $\phi_k(t)$ , and their corresponding eigenvalues  $\lambda_k$  are found by solving the functional eigenvalue problem:

$$\int_a^b C(s, t) \phi_k(t) dt = \lambda_k \phi_k(s). \quad (24)$$

## B Tables

Table B1: Descriptive statistics of each group

N = 64		Region							
		CEA	CWP	MID	SEA	SPL	SWP		
Group-1	Mean ± SD	507 ± 98	245 ± 73	618 ± 109	1178 ± 110	795 ± 90	892 ± 105		
	Min.	326	85	356	929	527	697		
	Max.	704	428	839	1465	1017	1145		
T90	Mean ± SD	0.44 ± 1.22	0.53 ± 1.33	0.01 ± 0.89	0.58 ± 1.23	0.58 ± 1.44	1.14 ± 1.78		
	Min.	-1.48	-1.65	-1.31	-1.24	-1.61	-1.91		
	Max.	3.57	5.15	3.57	4.48	5.32	5.87		
Group-2	Mean ± SD	3266 ± 281	2723 ± 186	3647 ± 337	1874 ± 237	3339 ± 274	2372 ± 167		
	Min.	2715	2285	2901	1416	2797	2025		
	Max.	3832	3238	4382	2452	4209	2799		
T10	Mean ± SD	-0.49 ± 1.06	-0.17 ± 0.90	-0.32 ± 0.97	-0.47 ± 0.98	-0.30 ± 0.93	-0.33 ± 0.89		
	Min.	-2.11	-1.50	-1.81	-1.84	-1.86	-1.84		
	Max.	1.98	2.42	2.41	2.49	2.88	2.51		
Group-3	Mean ± SD	11.35 ± 2.23	8.30 ± 1.86	10.12 ± 1.75	13.52 ± 2.61	7.04 ± 1.19	3.61 ± 1.04		
	Min.	6.80	3.88	6.11	7.50	4.49	1.55		
	Max.	19.04	13.50	13.82	20.38	10.21	7.02		
P	Mean ± SD	0.12 ± 1.01	0.60 ± 1.17	0.29 ± 1.05	-0.02 ± 0.93	0.35 ± 1.38	0.20 ± 0.97		
	Min.	-2.06	-1.43	-2.13	-2.07	-1.65	-1.92		
	Max.	3.48	2.84	2.95	1.85	5.26	2.93		

Note. N: Number of observations (years), SD: Standard deviation, Min: Minimum, Max: Maximum.



Table B3: MAPE values of GAM for each crop, model, and region

Set	Crop	Region	Model																						
			1	2	3	4	5	6	7	8	9	10	11	12	13	14	15	16	17	18	19	20	21	22	
Train	Corn	CEA	0.345	0.342	0.350	0.343	0.347	0.344	0.344	0.343	0.343	0.347	0.343	0.348	0.345	0.345	0.343	0.343	0.342	0.345	0.342	0.342	0.343	0.343	0.342
		CWP	0.388	0.393	0.396	0.391	0.393	0.397	0.395	0.391	0.394	0.399	0.392	0.397	0.399	0.397	0.397	0.398	0.397	0.399	0.397	0.399	0.398	0.396	0.396
		MID	0.357	0.355	0.360	0.355	0.357	0.356	0.358	0.355	0.357	0.357	0.357	0.357	0.358	0.355	0.355	0.354	0.355	0.355	0.354	0.355	0.354	0.354	0.355
		SEA	0.539	0.544	0.552	0.538	0.544	0.548	0.541	0.541	0.541	0.550	0.538	0.547	0.550	0.547	0.540	0.543	0.537	0.541	0.539	0.539	0.539	0.542	0.540
		SPL	0.204	0.261	0.252	0.256	0.218	0.220	0.225	0.257	0.219	0.187	0.233	0.233	0.220	0.196	0.208	0.220	0.109	0.228	0.073	0.107	0.107	0.119	0.188
		SWP	0.326	0.280	0.336	0.260	0.212	0.174	0.225	0.215	0.277	0.270	0.151	0.186	0.212	0.192	0.255	0.189	0.213	0.174	0.167	0.143	0.130	0.229	0.229
	Wheat	CEA	0.327	0.327	0.327	0.327	0.327	0.327	0.328	0.328	0.327	0.327	0.327	0.329	0.328	0.330	0.325	0.330	0.328	0.327	0.328	0.326	0.325	0.325	0.326
		CWP	0.242	0.238	0.254	0.256	0.251	0.258	0.249	0.250	0.249	0.246	0.254	0.244	0.250	0.241	0.250	0.251	0.248	0.251	0.251	0.251	0.251	0.248	0.250
		MID	0.335	0.334	0.334	0.334	0.334	0.335	0.333	0.334	0.334	0.333	0.335	0.335	0.334	0.343	0.346	0.347	0.345	0.348	0.346	0.345	0.344	0.342	0.345
		SEA	0.344	0.343	0.343	0.341	0.342	0.346	0.346	0.345	0.341	0.342	0.345	0.344	0.343	0.346	0.347	0.345	0.348	0.346	0.345	0.344	0.344	0.342	0.345
		SPL	0.214	0.222	0.218	0.217	0.217	0.221	0.222	0.221	0.218	0.220	0.224	0.222	0.218	0.220	0.214	0.219	0.216	0.219	0.217	0.217	0.216	0.215	0.224
		SWP	0.209	0.193	0.210	0.200	0.198	0.198	0.184	0.219	0.216	0.210	0.205	0.175	0.189	0.182	0.191	0.174	0.209	0.184	0.207	0.198	0.190	0.223	0.223
Test	Corn	CEA	0.324	0.325	0.312	0.322	0.308	0.304	0.305	0.322	0.321	0.307	0.318	0.309	0.311	0.309	0.308	0.306	0.314	0.307	0.314	0.307	0.305	0.313	
		CWP	0.293	0.293	0.293	0.292	0.294	0.293	0.294	0.292	0.294	0.293	0.293	0.294	0.293	0.293	0.292	0.292	0.293	0.291	0.293	0.292	0.291	0.292	
		MID	0.248	0.245	0.248	0.245	0.250	0.247	0.246	0.244	0.245	0.240	0.242	0.246	0.246	0.246	0.244	0.243	0.242	0.243	0.242	0.242	0.242	0.242	
		SEA	0.608	0.591	0.532	0.615	0.592	0.571	0.594	0.599	0.596	0.538	0.595	0.598	0.562	0.568	0.602	0.646	0.621	0.576	0.609	0.618	0.615	0.715	
		SPL	0.624	0.622	0.611	0.614	0.623	0.618	0.612	0.632	0.617	0.598	0.630	0.614	0.607	0.611	0.593	0.600	0.596	0.597	0.606	0.603	0.594	0.619	
		SWP	0.585	0.588	0.565	0.591	0.598	0.587	0.597	0.602	0.594	0.583	0.602	0.588	0.581	0.587	0.618	0.587	0.587	0.587	0.581	0.618	0.587	0.581	0.593
	Wheat	CEA	0.805	0.779	0.746	0.811	0.779	0.750	0.776	0.813	0.791	0.739	0.804	0.773	0.763	0.779	0.790	0.783	0.796	0.768	0.753	0.767	0.782	0.796	
		CWP	0.233	0.261	0.307	0.257	0.312	0.275	0.230	0.254	0.267	0.295	0.266	0.246	0.295	0.283	0.257	0.224	0.103	0.242	0.225	0.110	0.121	0.119	
		MID	0.210	0.169	0.359	0.162	0.200	0.208	0.162	0.228	0.185	0.281	0.290	0.249	0.185	0.173	0.159	0.211	0.124	0.210	0.119	0.168	0.235	0.264	
		SEA	0.605	0.535	0.542	0.519	0.550	0.543	0.546	0.533	0.534	0.546	0.530	0.539	0.540	0.548	0.590	0.552	0.535	0.547	0.558	0.542	0.525	0.538	
		SPL	0.423	0.408	0.416	0.393	0.423	0.401	0.397	0.435	0.409	0.388	0.416	0.395	0.365	0.366	0.373	0.384	0.374	0.391	0.370	0.364	0.396	0.401	
		SWP	0.524	0.539	0.564	0.529	0.542	0.562	0.555	0.543	0.545	0.561	0.528	0.542	0.560	0.557	0.568	0.562	0.557	0.560	0.568	0.562	0.560	0.539	
Soybeans	CEA	0.628	0.606	0.567	0.616	0.612	0.590	0.608	0.609	0.606	0.580	0.607	0.596	0.586	0.617	0.595	0.596	0.576	0.601	0.613	0.871	0.614	0.596		
	CWP	0.371	0.381	0.363	0.386	0.342	0.371	0.370	0.385	0.381	0.376	0.370	0.363	0.376	0.384	0.392	0.381	0.364	0.389	0.367	0.366	0.408	0.365		
	MID	0.517	0.505	0.478	0.521	0.502	0.500	0.521	0.516	0.509	0.487	0.504	0.508	0.528	0.497	0.561	0.537	0.520	0.556	0.552	0.540	0.547	0.520		
	SEA	0.482	0.494	0.498	0.492	0.473	0.495	0.495	0.492	0.495	0.486	0.498	0.485	0.488	0.486	0.487	0.480	0.486	0.485	0.487	0.480	0.485	0.507		
	SPL	0.580	0.571	0.491	0.609	0.539	0.518	0.540	0.611	0.580	0.495	0.590	0.561	0.532	0.565	0.528	0.564	0.593	0.577	0.577	0.562	0.599	0.600		
	SWP	0.455	0.451	0.440	0.444	0.439	0.434	0.418	0.462	0.431	0.429	0.469	0.471	0.418	0.432	0.415	0.399	0.442	0.417	0.441	0.453	0.433	0.461		

Table B4: MAPE values of XGB for each crop, model, and region

Set	Crop	Region	Model																						
			1	2	3	4	5	6	7	8	9	10	11	12	13	14	15	16	17	18	19	20	21	22	
Train	Corn	CEA	0.047	0.053	0.044	0.051	0.042	0.047	0.043	0.038	0.046	0.048	0.042	0.039	0.055	0.043	0.047	0.039	0.048	0.044	0.044	0.044	0.040	0.041	0.053
		CWP	0.028	0.035	0.029	0.036	0.037	0.034	0.039	0.035	0.037	0.042	0.034	0.032	0.044	0.040	0.044	0.042	0.044	0.044	0.053	0.042	0.044	0.053	0.037
		MID	0.028	0.034	0.037	0.025	0.032	0.034	0.035	0.036	0.037	0.044	0.032	0.044	0.040	0.044	0.044	0.042	0.044	0.044	0.053	0.042	0.044	0.053	0.037
		SEA	0.037	0.057	0.054	0.035	0.036	0.047	0.040	0.040	0.040	0.058	0.055	0.043	0.046	0.046	0.049	0.053	0.053	0.043	0.043	0.051	0.056	0.047	0.043
	Wheat	SPL	0.137	0.146	0.160	0.139	0.147	0.135	0.122	0.132	0.166	0.130	0.127	0.157	0.127	0.130	0.124	0.116	0.118	0.062	0.137	0.058	0.061	0.066	0.116
		SWP	0.137	0.154	0.151	0.162	0.133	0.090	0.123	0.134	0.155	0.145	0.126	0.110	0.098	0.088	0.139	0.088	0.139	0.088	0.095	0.090	0.084	0.075	0.089
		CEA	0.038	0.035	0.032	0.035	0.035	0.029	0.032	0.040	0.031	0.038	0.039	0.035	0.034	0.029	0.035	0.035	0.033	0.031	0.041	0.037	0.033	0.036	0.037
		CWP	0.057	0.052	0.047	0.058	0.051	0.049	0.053	0.050	0.052	0.040	0.052	0.033	0.036	0.036	0.039	0.042	0.038	0.042	0.039	0.043	0.040	0.047	0.044
	Soybeans	MID	0.043	0.041	0.036	0.046	0.042	0.036	0.037	0.042	0.045	0.035	0.036	0.039	0.040	0.040	0.042	0.038	0.040	0.042	0.038	0.040	0.042	0.042	0.041
		SEA	0.044	0.047	0.045	0.039	0.038	0.031	0.032	0.047	0.048	0.051	0.051	0.043	0.046	0.041	0.045	0.039	0.033	0.039	0.044	0.039	0.044	0.039	0.043
		SPL	0.041	0.045	0.040	0.041	0.037	0.040	0.045	0.036	0.050	0.039	0.044	0.042	0.043	0.040	0.043	0.045	0.045	0.042	0.042	0.042	0.042	0.047	0.045
		SWP	0.063	0.061	0.054	0.069	0.063	0.053	0.044	0.064	0.061	0.055	0.068	0.041	0.043	0.043	0.051	0.050	0.038	0.051	0.042	0.049	0.044	0.048	0.057
Test	Corn	CEA	0.052	0.059	0.037	0.061	0.037	0.044	0.038	0.046	0.061	0.049	0.050	0.044	0.057	0.047	0.051	0.046	0.059	0.047	0.053	0.042	0.047	0.059	
		CWP	0.029	0.035	0.029	0.026	0.027	0.027	0.029	0.034	0.028	0.033	0.032	0.031	0.032	0.032	0.029	0.033	0.032	0.035	0.029	0.033	0.035	0.035	
		SEA	0.038	0.057	0.051	0.040	0.040	0.043	0.049	0.037	0.045	0.047	0.042	0.050	0.058	0.051	0.050	0.056	0.042	0.051	0.048	0.043	0.048	0.055	
		SPL	0.036	0.045	0.037	0.044	0.036	0.040	0.038	0.046	0.046	0.044	0.047	0.040	0.036	0.046	0.037	0.043	0.043	0.039	0.047	0.041	0.043	0.046	0.049
	Wheat	CEA	0.109	0.129	0.101	0.106	0.102	0.103	0.108	0.103	0.112	0.100	0.100	0.105	0.119	0.111	0.113	0.108	0.112	0.115	0.119	0.119	0.105	0.098	0.129
		CWP	0.043	0.049	0.038	0.044	0.041	0.042	0.042	0.037	0.042	0.038	0.042	0.037	0.037	0.039	0.040	0.043	0.039	0.049	0.045	0.043	0.041	0.046	
		MID	0.055	0.053	0.047	0.052	0.053	0.055	0.050	0.049	0.049	0.056	0.047	0.050	0.051	0.056	0.060	0.060	0.060	0.058	0.056	0.060	0.060	0.064	
		SEA	0.074	0.074	0.071	0.072	0.070	0.068	0.078	0.073	0.086	0.067	0.073	0.066	0.076	0.066	0.076	0.080	0.087	0.082	0.087	0.076	0.084	0.081	0.093
	Soybeans	SPL	0.235	0.273	0.293	0.239	0.256	0.268	0.230	0.277	0.271	0.292	0.247	0.258	0.246	0.230	0.258	0.242	0.099	0.258	0.082	0.097	0.119	0.152	
		SWP	0.163	0.186	0.306	0.129	0.162	0.174	0.157	0.144	0.184	0.285	0.124	0.135	0.157	0.114	0.155	0.178	0.112	0.176	0.119	0.148	0.179	0.179	
		CEA	0.059	0.060	0.067	0.065	0.068	0.068	0.070	0.069	0.053	0.067	0.066	0.060	0.062	0.071	0.075	0.059	0.053	0.079	0.053	0.079	0.074	0.065	
		CWP	0.102	0.090	0.103	0.115	0.107	0.085	0.093	0.081	0.094	0.094	0.089	0.095	0.095	0.086	0.094	0.092	0.100	0.086	0.092	0.105	0.086	0.099	
Wheat	MID	0.076	0.073	0.073	0.067	0.066	0.071	0.062	0.075	0.076	0.065	0.063	0.072	0.068	0.070	0.070	0.072	0.070	0.090	0.070	0.072	0.090	0.078		
	SEA	0.072	0.088	0.056	0.083	0.075	0.073	0.077	0.085	0.079	0.067	0.072	0.065	0.060	0.080	0.083	0.069	0.072	0.076	0.070	0.078	0.084	0.075		
	SPL	0.094	0.089	0.083	0.083	0.084	0.081	0.073	0.087	0.072	0.073	0.086	0.092	0.077	0.087	0.081	0.078	0.080	0.077	0.062	0.088	0.083	0.096		
	SWP	0.154	0.151	0.139	0.154	0.159	0.146	0.148	0.156	0.149	0.136	0.147	0.160	0.139	0.141	0.150	0.157	0.148	0.146	0.144	0.157	0.154	0.172		
Soybeans	CEA	0.105	0.116	0.085	0.107	0.083	0.094	0.103	0.098	0.116	0.107	0.097	0.102	0.106	0.104	0.102	0.112	0.086	0.097	0.101	0.101	0.098	0.114		
	MID	0.061	0.058	0.047	0.064	0.046	0.047	0.053	0.056	0.057	0.052	0.059	0.045	0.059	0.053	0.052	0.052	0.046	0.059	0.052	0.052	0.059	0.056		
	SEA	0.103	0.133	0.101	0.123	0.102	0.101	0.093	0.112	0.109	0.099	0.120	0.106	0.117	0.102	0.110	0.104	0.096	0.092	0.109	0.100	0.111	0.128		
	SPL	0.077	0.094	0.076	0.078	0.076	0.085	0.082	0.070	0.086	0.070	0.077	0.076	0.075	0.067	0.059	0.063	0.070	0.071	0.088	0.067	0.071	0.084		

Table B5: MAPE values of LGBM for each crop, model, and region

Set	Crop	Region	Model																						
			1	2	3	4	5	6	7	8	9	10	11	12	13	14	15	16	17	18	19	20	21	22	
Train	Corn	CEA	0.093	0.100	0.088	0.095	0.083	0.098	0.087	0.086	0.095	0.094	0.089	0.093	0.091	0.092	0.093	0.086	0.094	0.086	0.094	0.086	0.094	0.094	0.100
		CWP	0.067	0.064	0.064	0.064	0.063	0.063	0.065	0.063	0.063	0.065	0.065	0.062	0.062	0.062	0.059	0.063	0.061	0.065	0.065	0.059	0.065	0.065	0.060
		MID	0.076	0.080	0.085	0.073	0.078	0.081	0.076	0.078	0.081	0.077	0.083	0.085	0.085	0.085	0.083	0.080	0.085	0.087	0.083	0.083	0.080	0.087	0.082
		SEA	0.105	0.111	0.111	0.097	0.103	0.107	0.109	0.104	0.113	0.116	0.116	0.107	0.101	0.109	0.110	0.107	0.103	0.105	0.109	0.102	0.097	0.116	0.116
	Wheat	SPL	0.280	0.286	0.295	0.285	0.296	0.273	0.287	0.280	0.271	0.286	0.274	0.269	0.262	0.264	0.274	0.208	0.268	0.206	0.220	0.214	0.249	0.249	
		SWP	0.302	0.326	0.352	0.307	0.319	0.297	0.296	0.304	0.336	0.345	0.304	0.284	0.274	0.292	0.293	0.275	0.237	0.299	0.283	0.262	0.302	0.302	
		CEA	0.071	0.070	0.066	0.071	0.063	0.062	0.063	0.069	0.071	0.066	0.068	0.066	0.068	0.064	0.066	0.067	0.066	0.069	0.068	0.071	0.069	0.070	
		CWP	0.106	0.097	0.098	0.103	0.103	0.094	0.100	0.096	0.101	0.081	0.095	0.082	0.082	0.093	0.089	0.091	0.092	0.091	0.090	0.092	0.100	0.097	
	Soybeans	MID	0.078	0.078	0.072	0.077	0.076	0.072	0.072	0.079	0.078	0.074	0.078	0.077	0.074	0.075	0.079	0.071	0.075	0.074	0.079	0.071	0.074	0.076	
		SEA	0.087	0.092	0.084	0.090	0.085	0.083	0.080	0.092	0.090	0.093	0.091	0.083	0.088	0.086	0.088	0.086	0.089	0.083	0.091	0.084	0.085	0.092	
		SPL	0.075	0.077	0.075	0.074	0.073	0.072	0.075	0.078	0.078	0.075	0.076	0.074	0.076	0.074	0.075	0.073	0.074	0.076	0.074	0.076	0.075	0.078	
		SWP	0.118	0.120	0.122	0.116	0.118	0.116	0.115	0.121	0.119	0.119	0.119	0.113	0.112	0.115	0.112	0.113	0.108	0.100	0.109	0.108	0.110	0.120	
Test	Corn	CEA	0.101	0.104	0.091	0.101	0.092	0.094	0.091	0.094	0.101	0.095	0.097	0.096	0.096	0.097	0.100	0.098	0.098	0.098	0.094	0.097	0.104	0.104	
		CWP	0.057	0.062	0.055	0.060	0.056	0.055	0.058	0.058	0.059	0.058	0.059	0.058	0.058	0.061	0.057	0.060	0.061	0.059	0.057	0.060	0.059	0.060	
		SEA	0.100	0.112	0.115	0.102	0.106	0.110	0.110	0.103	0.106	0.120	0.105	0.107	0.116	0.114	0.116	0.115	0.102	0.111	0.110	0.106	0.109	0.115	
		SPL	0.079	0.082	0.077	0.081	0.074	0.084	0.079	0.083	0.083	0.083	0.081	0.080	0.075	0.081	0.082	0.082	0.083	0.085	0.082	0.086	0.084	0.083	
	Wheat	CEA	0.111	0.112	0.100	0.117	0.101	0.105	0.102	0.115	0.107	0.101	0.110	0.100	0.109	0.116	0.112	0.114	0.113	0.114	0.103	0.105	0.110	0.110	
		CWP	0.035	0.034	0.037	0.037	0.037	0.036	0.036	0.035	0.036	0.040	0.036	0.039	0.038	0.036	0.036	0.035	0.039	0.037	0.038	0.036	0.034	0.038	
		MID	0.055	0.052	0.051	0.048	0.047	0.047	0.052	0.052	0.054	0.052	0.055	0.049	0.055	0.054	0.053	0.055	0.053	0.053	0.054	0.055	0.053	0.054	
		SEA	0.071	0.079	0.069	0.079	0.072	0.068	0.075	0.079	0.081	0.077	0.078	0.079	0.073	0.078	0.080	0.074	0.079	0.073	0.073	0.072	0.074	0.087	
	Soybeans	SPL	0.270	0.290	0.293	0.274	0.278	0.287	0.261	0.266	0.255	0.287	0.273	0.267	0.264	0.261	0.282	0.274	0.187	0.282	0.187	0.195	0.206	0.220	
		SWP	0.198	0.226	0.298	0.200	0.230	0.249	0.226	0.194	0.234	0.287	0.187	0.227	0.263	0.210	0.235	0.238	0.203	0.230	0.164	0.214	0.230	0.214	
		CEA	0.067	0.063	0.066	0.061	0.065	0.066	0.066	0.065	0.066	0.064	0.063	0.064	0.062	0.059	0.063	0.061	0.061	0.064	0.065	0.062	0.064	0.066	
		CWP	0.090	0.093	0.099	0.101	0.093	0.094	0.095	0.097	0.102	0.106	0.098	0.099	0.100	0.112	0.106	0.103	0.105	0.101	0.090	0.100	0.100	0.103	
Soybeans	MID	0.066	0.069	0.066	0.067	0.072	0.066	0.061	0.067	0.064	0.068	0.067	0.069	0.069	0.066	0.066	0.065	0.066	0.072	0.069	0.065	0.071	0.072		
	SEA	0.065	0.067	0.067	0.062	0.061	0.065	0.064	0.065	0.068	0.064	0.065	0.073	0.063	0.060	0.065	0.070	0.062	0.067	0.059	0.068	0.068	0.068		
	SPL	0.079	0.077	0.075	0.073	0.074	0.070	0.071	0.077	0.069	0.070	0.076	0.070	0.074	0.066	0.073	0.072	0.075	0.075	0.074	0.075	0.078	0.079		
	SWP	0.164	0.148	0.160	0.157	0.159	0.151	0.153	0.159	0.152	0.157	0.151	0.142	0.142	0.151	0.151	0.151	0.151	0.149	0.146	0.168	0.164	0.176		
Soybeans	CEA	0.101	0.102	0.100	0.103	0.090	0.099	0.091	0.103	0.101	0.093	0.104	0.101	0.094	0.101	0.105	0.104	0.091	0.107	0.106	0.101	0.105	0.097		
	MID	0.055	0.053	0.047	0.053	0.052	0.051	0.054	0.053	0.051	0.054	0.050	0.054	0.049	0.051	0.050	0.054	0.042	0.051	0.050	0.054	0.051	0.052		
	SEA	0.116	0.129	0.109	0.129	0.114	0.123	0.119	0.129	0.136	0.114	0.129	0.116	0.126	0.129	0.119	0.123	0.110	0.106	0.125	0.131	0.126	0.137		
	SPL	0.079	0.081	0.076	0.077	0.079	0.073	0.076	0.080	0.083	0.073	0.077	0.079	0.083	0.075	0.080	0.073	0.081	0.081	0.078	0.078	0.073	0.079		

Table B6: MAPE values of XGB-C for each crop, model, and region

Set	Crop	Region	Model																							
			1	2	3	4	5	6	7	8	9	10	11	12	13	14	15	16	17	18	19	20	21	22		
Train	Corn	CEA	0.051	0.054	0.047	0.040	0.032	0.034	0.029	0.040	0.055	0.056	0.034	0.030	0.039	0.029	0.029	0.029	0.029	0.028	0.029	0.029	0.028	0.028	0.053	
		CWP	0.045	0.033	0.035	0.031	0.028	0.028	0.028	0.037	0.038	0.027	0.030	0.025	0.024	0.022	0.021	0.022	0.022	0.019	0.021	0.019	0.018	0.018	0.032	
		MID	0.032	0.036	0.038	0.025	0.022	0.020	0.020	0.036	0.034	0.045	0.024	0.027	0.030	0.021	0.020	0.021	0.020	0.021	0.020	0.020	0.020	0.021	0.020	0.038
		SEA	0.039	0.062	0.051	0.035	0.027	0.041	0.025	0.042	0.062	0.049	0.037	0.035	0.039	0.031	0.028	0.028	0.027	0.027	0.025	0.025	0.024	0.023	0.023	0.057
	Wheat	SPL	0.133	0.134	0.161	0.090	0.105	0.113	0.082	0.160	0.152	0.129	0.134	0.090	0.100	0.080	0.072	0.078	0.033	0.033	0.072	0.031	0.032	0.030	0.100	
		SWP	0.151	0.152	0.191	0.113	0.090	0.098	0.080	0.134	0.154	0.145	0.114	0.082	0.091	0.072	0.067	0.052	0.050	0.051	0.049	0.044	0.044	0.044	0.146	
		CEA	0.037	0.040	0.036	0.030	0.027	0.026	0.023	0.035	0.049	0.033	0.031	0.024	0.028	0.024	0.023	0.023	0.023	0.022	0.022	0.022	0.021	0.020	0.041	
		CWP	0.066	0.051	0.047	0.046	0.043	0.034	0.033	0.049	0.048	0.034	0.037	0.026	0.025	0.021	0.020	0.021	0.020	0.019	0.019	0.019	0.019	0.018	0.043	
	Soybeans	MID	0.043	0.043	0.038	0.038	0.032	0.033	0.026	0.041	0.049	0.038	0.039	0.031	0.034	0.030	0.028	0.027	0.030	0.025	0.028	0.027	0.025	0.025	0.044	
		SEA	0.042	0.047	0.036	0.036	0.028	0.026	0.024	0.052	0.043	0.045	0.036	0.035	0.036	0.030	0.028	0.023	0.026	0.022	0.022	0.025	0.022	0.021	0.050	
		SPL	0.041	0.047	0.039	0.036	0.030	0.034	0.027	0.040	0.041	0.043	0.030	0.034	0.035	0.027	0.026	0.024	0.028	0.022	0.022	0.025	0.025	0.022	0.046	
		SWP	0.067	0.057	0.056	0.046	0.042	0.037	0.032	0.066	0.055	0.042	0.050	0.033	0.037	0.032	0.027	0.023	0.021	0.021	0.020	0.019	0.018	0.018	0.068	
Test	Corn	CEA	0.059	0.052	0.045	0.044	0.036	0.035	0.033	0.050	0.058	0.057	0.042	0.040	0.045	0.035	0.033	0.031	0.032	0.031	0.032	0.031	0.032	0.029	0.060	
		CWP	0.037	0.034	0.029	0.030	0.024	0.024	0.023	0.031	0.026	0.031	0.024	0.023	0.024	0.020	0.017	0.020	0.020	0.017	0.017	0.017	0.020	0.017	0.030	
		SEA	0.040	0.059	0.049	0.035	0.029	0.033	0.026	0.041	0.058	0.054	0.029	0.034	0.036	0.025	0.024	0.024	0.020	0.020	0.022	0.019	0.019	0.019	0.054	
		SPL	0.036	0.043	0.035	0.027	0.025	0.026	0.023	0.044	0.044	0.046	0.032	0.037	0.034	0.027	0.022	0.022	0.023	0.023	0.022	0.022	0.022	0.023	0.054	
	Wheat	CEA	0.109	0.119	0.087	0.101	0.093	0.108	0.093	0.107	0.108	0.104	0.102	0.096	0.113	0.103	0.104	0.104	0.101	0.106	0.099	0.102	0.099	0.102	0.109	
		CWP	0.044	0.046	0.040	0.047	0.043	0.039	0.041	0.037	0.040	0.043	0.041	0.045	0.043	0.044	0.045	0.045	0.046	0.048	0.045	0.044	0.044	0.044	0.049	
		MID	0.047	0.059	0.045	0.048	0.042	0.051	0.045	0.043	0.049	0.049	0.044	0.042	0.043	0.042	0.046	0.042	0.046	0.046	0.046	0.046	0.042	0.042	0.058	
		SEA	0.068	0.089	0.075	0.070	0.066	0.074	0.065	0.074	0.088	0.080	0.073	0.069	0.071	0.069	0.067	0.072	0.073	0.071	0.073	0.072	0.072	0.072	0.086	
	Soybeans	SPL	0.210	0.315	0.317	0.233	0.223	0.294	0.236	0.254	0.281	0.275	0.272	0.239	0.221	0.228	0.246	0.237	0.102	0.249	0.089	0.095	0.084	0.107		
		SWP	0.137	0.176	0.332	0.141	0.151	0.187	0.154	0.095	0.192	0.291	0.104	0.140	0.189	0.144	0.150	0.190	0.157	0.187	0.115	0.115	0.157	0.111	0.169	
		CEA	0.066	0.067	0.062	0.069	0.063	0.057	0.059	0.068	0.063	0.069	0.066	0.067	0.060	0.063	0.066	0.064	0.066	0.063	0.063	0.063	0.068	0.060	0.066	
		CWP	0.102	0.087	0.094	0.093	0.086	0.081	0.086	0.082	0.092	0.091	0.080	0.078	0.084	0.079	0.079	0.079	0.079	0.074	0.079	0.079	0.076	0.079	0.091	